NON-INVASIVE ESTIMATION OF LITHIUM-ION CELL THERMO-PHYSICAL PROPERTIES

A Thesis

by

KARAN NARULA

Submitted to the Office of Graduate and Professional Studies of
Texas A&M University
in partial fulfillment of the requirements for the degree of

MASTER OF SCIENCE

Chair of Committee,	Partha P. Mukherjee
Committee Members,	Waruna Kulatilaka
	Sarbajit Banerjee
Head of Department,	Andreas Polycarpou

May 2017

Major Subject: Mechanical Engineering

ABSTRACT

Cylindrical Li-ion cells have one of the highest energy density and power density of all Li-ion cell types and typically employ a spiral electrode assembly. This spiral assembly leads to a large anisotropy leading to a drastic difference in the thermo-physical properties in the axial and the radial direction. The radial direction has multiple layers of electrodes and separators leading to a high thermal impedance in this direction, whereas in the axial direction, not many obstacles are present and hence the thermal conductivity is on the higher side. This research describes a novel experimental technique to measure the anisotropic thermal conductivity and heat capacity of Li-ion cells using thermal impedance spectroscopy (T.I.S). It is paramount to experimentally measure the radial and axial thermal conductivities of a cylindrical Li-ion cell because the assumption of isotropic thermal transport properties in Li-ion cell design would lead us to either under predict the value or over predict the value of the temperature field - both of which would lead to highly undesirable results.

The experimental measurements indicate that radial thermal conductivity is two orders of magnitude lower than axial thermal conductivity for cylindrical 18650 cells which is in sync to what we intuited. Moreover, the work presented here also establishes a trend of the change in thermos-physical properties with varying the state of charge of the cell. This is extremely helpful in order to develop an efficient cooling system for any device that needs to continuously charge and discharge over thousands of cycles. The data helps to

account for the change in the thermal conductivity and heat capacity over a period of cycling of the cell and thus encouraging an update in the cooling system for the device also in order to avoid hazardous situations such as thermal runaway.

Lastly, the technique presented in this research is a non-invasive, robust, quick and extremely economical way to determine the thermos-physical properties of an 18650 lithium-ion cell. It also determines the change in thermos-physical properties with the changing state of health of the cell.

DEDICATION

First and foremost, I would like to dedicate this thesis to my advisor, Dr. Partha Mukherjee, who has been a constant source of support and encouragement during the times when things looked bleak.

I dedicate this to my group Ph.D. members, Aashutosh Mistry and Daniel Robles Juarez, for the deft ways in which they lovingly challenged and supported me throughout the whole of this journey and helped me to find and realize my potential.

This thesis is also dedicated to my father, who has been my source of inspiration, and to my mother, who taught me that even the largest task can be accomplished if done one step at a time.

Lastly, this thesis is dedicated to all these people without whom this could not have been possible.

ACKNOWLEDGEMENTS

Foremost, I would like to express my sincere gratitude to Dr. Partha Mukherjee, Dr. Waruna Kulatilaka (committee member) and Dr. Sarbajit Banerjee (committee member) for their support, patience, motivation and immense knowledge. Their guidance greatly helped me in the time of research and during the writing of this thesis.

I would also like to thank Aashutosh Mistry and Daniel Robles Juarez for their insightful thoughts, comments and monumental encouragement at every step and for being more than generous with their expertise and precious time.

I would like to acknowledge and thank the Energy and Transport Sciences Lab at the Texas A&M University for allowing me to conduct my research and providing assistance in any form as requested.

Finally, I wish to extend my heartfelt gratitude towards my parents for providing me with unfailing support and continuous encouragement throughout my years of study and through the process of researching and writing this thesis.

Thank you.

CONTRIBUTORS AND FUNDING SOURCES

This work was supervised by Dr. Partha Mukherjee. Dr. Waruna Kulatilaka of the Department of Mechanical Engineering and Dr. Sarbajit Banerjee of the Department of Chemistry were members of the thesis committee.

All work for the thesis was completed independently by the student.

This research was supported in part by the faculty research initiation grant from Texas A&M University.

TABLE OF CONTENTS

Page

LIST OF FIGURES

Page

LIST OF TABLES

Page

CHAPTER I

INTRODUCTION

Need for energy storage

There is a dire need for our society as a whole to move towards cleaner, more efficient and more renewable energy sources. The extinct of non-renewable energy sources is near. Oil, petroleum and other minerals are predicted to get extinct in the near future. The one crucial component that is typically overlooked in the energy technology conversation is the topic of energy storage. There have been significant improvements in solar and wind energy and this is critical in the battle against climate change, but without any further improvements in energy storage, our efforts will fall short. We will face serious energy needs and requirements in situations when the sun isn't shining or the wind isn't blowing? There are various ways to store energy such as flywheels, ultra-capacitors, and compressed air but batteries are the best choice for almost all applications. Batteries can be of various sizes ranging from small batteries used in watches, cell phone and calculators, to medium batteries used in pure Electric Vehicles (EVs), Hybrid Electric Vehicles (HEVs), to large batteries used to power submarines or for signal circuits or other long duration grid applications. They are highly efficient and profitable and have high energy-to-weight ratios. Energy storage is crucial to many applications, ranging from small-scale portable electronics to large-scale renewable energy sources. It is crucial that we receive reliable electricity supply 24 hours a day. But, it is difficult to just switch over to using solar and wind for all our energy needs because both the solar power and wind power are not always available when needed. The solution to this issue lies in energy storage. Storing this energy

generated from solar and wind power into reliable, powerful batteries is the key to the availability of energy whenever needed.

Energy storage radically betters the way we generate, transport, and exhaust energy in the form of electricity. Energy storage is instrumental during emergency situations like power outages from storms, equipment failures, accidents or even terrorist attacks. But the fascinating nature of energy storage is its ability to balance demand and power supply *instantaneously* which makes power networks more resilient, valuable, and cleaner than ever before.

Figure 1: Sony rechargeable battery (Reprinted from [1])

Nomenclature and types of batteries based on physical packaging

Glass jars were mostly used to encase the batteries in the early 1700s but as the size of batteries grew, sealed wooden containers and composite materials replaced jars. Battery sizes were hand-built for specific uses. When cells started to be used in portable electronic devices, sealed cylindrical cells emerged that led to standards.

Cells can be divided into the following four categories based on their packaging and shapes:

- Cylindrical Cells
- Coin Cells
- Prismatic Cells
- Pouch Cells

Cylindrical cell

The cylindrical cell is one of the most widely used packaging styles for primary and

Figure 2: 18650 Cylindrical lithium-ion cells

secondary batteries. The first two digits of 18650 designate the diameter in millimeters and the next three digits are the length in the tenths of millimeters. The 18650 cells is 18mm in diameter and 65.0mm in length. The ease of manufacturing and good mechanical

stability is a few of its advantages. The tubular cylindrical cell can also withstand high internal pressures without deforming which adds to its list of advantages. Typical applications for the cylindrical cell are power tools, medical instruments, laptops and e-bikes and even Electric Vehicles (EVs) and Hybrid Electrical Vehicles (HEVs).

Coin cell

The coin cell has enabled and made it possible for everyone to be used in portable devices since the 1980s. High voltages are achieved by stacking the cells into a tube. These cells are used in cordless telephones, medical devices and security wands at airports. A major drawback of the coin cell is swelling if it is charged too rapidly. These cells have no safety vent and most button cells in use today are non-rechargeable in nature and are found in medical implants, watches, hearing aids, car keys and memory backup.

Figure 3: Coin cell

Prismatic cell

Prismatic cells were developed in the 1990s so as to meet the requirements of thinner sized cells and lower manufacturing costs of cells. Prismatic cells use the first two digits to

indicate the thickness in the tenth of millimeters. The next two digits designate the widths and the last two provide the length of the cell in millimeters. The 533545P prismatic cell, for example, is 5.3mm thick, 35mm wide and 54mm long. P stands for prismatic. To increase the volume density of the battery pack, the layered approach is used where-in multiple layers of the cathode and the anode are present in the cell. Prismatic cells are predominantly used in mobile phones and laptops because they have the highest energy density, which means more increased capacity for the same size of cell and consequentially increased hours of mobile phone usage.

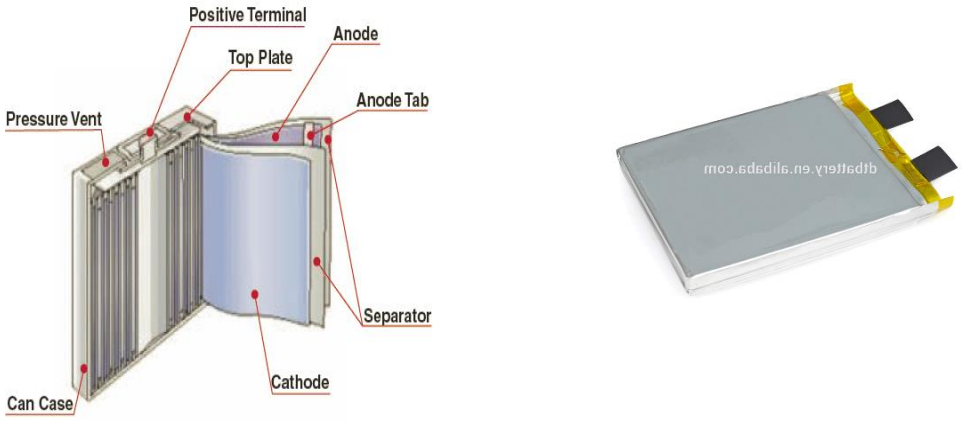

[a] [b]

Figure 4: [a] Cross-section view of prismatic cell (Reprinted from [2]), [b] prismatic cell (Reprinted from [3])

Pouch cell

The invention of pouch cells startled everyone because of its unique and exclusive design. The structure of these cells involves conductive foil tabs, which are welded to the electrode and sealed to the pouch so as to carry the positive and negative terminals to the outside instead of using a metallic cylinder and glass-to-metal electrical feed-through for insulation. The pouch cell makes the most valuable use of space and achieves a 95 percent packaging efficiency, the highest among battery packs. These pouch cells are used in military applications, as well as automotive applications.

Figure 5: Coin cell (Reprinted from [4])

Working of li-ion battery

A battery is a device that stores electrical energy and can then deliver that energy through an easily controlled electrochemical reaction [5]. A battery is usually composed of a series of cells, connect in series or parallel that produce electricity. Each cell has three essential components: the anode, the cathode, and the electrolyte. When an electrical conductor like a wire connects the anode and cathode, electrons flow from the anode through the wire to the cathode, creating an electrical current, while the electrolyte conducts ions.

The cathode and anode materials are selected so that the anode donates electrons, and the cathode accepts them. The ability of a material to donate or accept electrons is commonly expressed in terms of the material's standard electrode potential. The difference between the electrode potential of the anode and the cathode determines the voltage of the entire cell. The electrolyte, which is a liquid or gel separates the cathode and anode. It acts as an excellent ionic current conductor and an excellent electronic current insulator. Once the anode and cathode are connected in the circuit, the anode undergoes a chemical reaction with the electrolyte in which it loses electrons, creating cations, or positive ions, a process called oxidation. The electrons and cations meet at the cathode where they undergo a chemical reaction called reduction. This entire process of accepting and donating electrons is known as a reduction-oxidation, or redox, reaction. The electrons, during the discharge of the battery travel through the external wire from the anode to cathode and in the reverse direction during charging of the battery.

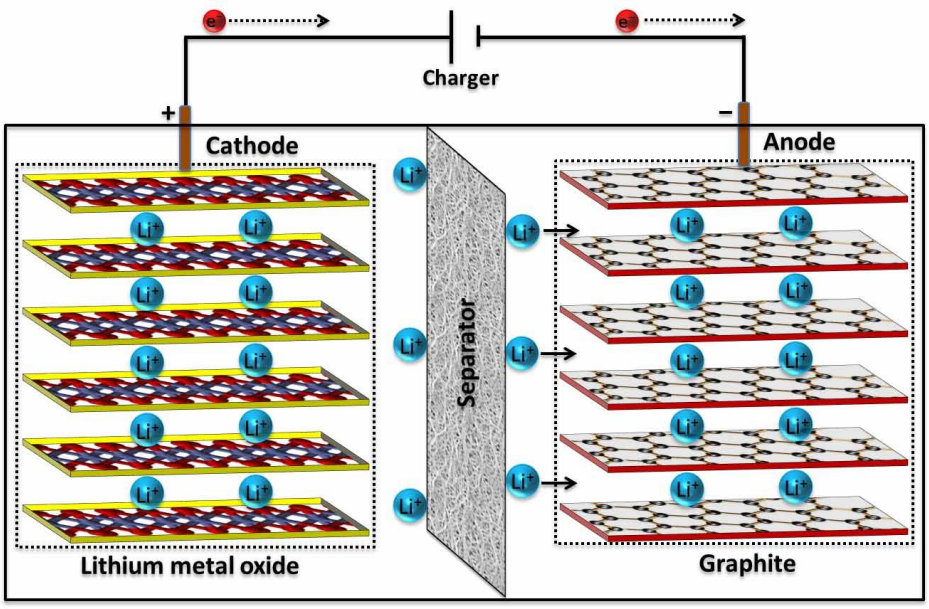

Figure 6: Working of lithium-ion battery (Reprinted from [6])

The anode of a conventional lithium ion cell is made from carbon, a metal oxide usually acts like a cathode, and the electrolyte is a lithium salt in an organic solvent. Graphite is the most commercially popular material which is used for the anode. Graphite is a crystalline solid with a black or grey color and a metallic sheen. It is highly conductive due to its electronic structure, and can reach 25,000 S/cm2 in the plane of a single-crystal. Graphite is used as the active material in negative electrodes mainly because it can reversibly allow lithium-ions between its many layers. This reversible electrochemical capability is maintained over several of thousands of cycles in batteries with optimized electrodes. The cathode of the cell can be one of three materials namely a polyanion such as lithium iron phosphate or a layered oxide (such as lithium cobalt oxide), or a spinel

such as lithium manganese oxide. A mixture of organic carbonates such as ethylene carbonate (EC) or diethyl carbonate (DEC) containing other complex compounds is usually used as a solvent. Non-coordinating anion salts such as lithium perchlorate ($LiClO_4$), lithium tetrafluoroborate ($LiBF_4$) lithium hexafluorophosphate ($LiPF_6$) and lithium hexafluoroarsenate monohydrate ($LiAsF_6$), are used by non-aqueous electrolytes. The separator is a very thin sheet of micro-perforated plastic which is necessary to separate the anode from the cathode in order to avoid shorting of the cell. It is located between the cathode and the anode and separates the positive and negative electrodes while allowing ions to pass through.

While charging, lithium ions move from its cathode towards the anode. During this process, intercalation of the lithium ions takes place inside the graphite anode, while the electrons flow in through an external electrical circuit from the cathode to the anode. During the discharge process, the lithium ions in the graphite de-intercalate and move towards the cathode, while the device being charged in the process of moving from anode to cathode uses the electrons in the external wire. A lithium ion battery is also known as a swing battery or rocking chair battery since two-way movement of lithium ions between anode and cathode through the electrolyte occurs during charge and discharge process. The more lithium the electrodes can take in, the more total energy the battery can store, and the longer it can last. Most types of batteries are based on the $C/LiPF_6$ in EC–$DMC/LiMO_2$ sequence.

The reactions inside the li-ion cell can be represented as follows:

Positive electrode (cathode) reduction reaction

$$CoO2 + xLi+ + xe- \rightarrow LiCoO2$$

Negative Electrode (anode) oxidation reaction

$$LiC6 \rightarrow xLi+ + xC6 + e-$$

Overall reversible, Redox, cell reaction

$$LiC6 + CoO2 \rightarrow C6 + LiCoO2$$

Advantages and disadvantages of li-ion batteries

Lithium-ion batteries like any other technology have their set of advantages and disadvantages. These batteries are currently very famous and its advantages supersede its disadvantages by a large margin.

Advantages

Some of the major advantages of lithium-ion batteries are as follows [7]:

High energy density

Lithium ion batteries or cells have one of the largest energy densities as compared to all other batteries. A lot of energy can be stored in the atomic bonds of lithium as it is a highly reactive element. This leads to the dramatically high energy density of lithium-ion batteries and thus they can be used for large number of applications requiring the large energy density. Most of the electronic equipment nowadays needs to run for a long periods between subsequent charges. This includes small devices such as our mobiles phones or large electrical vehicles and hybrid electrical vehicles. Thus, there is an immense need to

develop batteries having large energy density so as to sustain the daily use of all the devices. The excessive power density offered by lithium ion batteries as compared to other batteries is a huge boon and is a distinct advantage.

Figure 7: Chevrolet Bolt's electric power train (Reprinted from [8])

Self-discharge

Most of the batteries and cell face the issue of losing charge over time without any usage. This issue is termed as self-discharge and is evident in all the batteries. It is one of the major issues faced by battery manufacturers as it significantly reduces the battery usage time. The major advantage of using lithium-ion batteries is that their self-discharge rate is significantly lower as compared to other rechargeable cells such as Ni-Cad and NiMH forms. Typically Ni/Cd and Ni/MH cells suffer self-discharge rates as high as 25% per month whereas Li-ion cells typically lose only 8% of their capacity for the first month and

then 2% for subsequent months which is significantly less as compared to the rest of the batteries. [9]

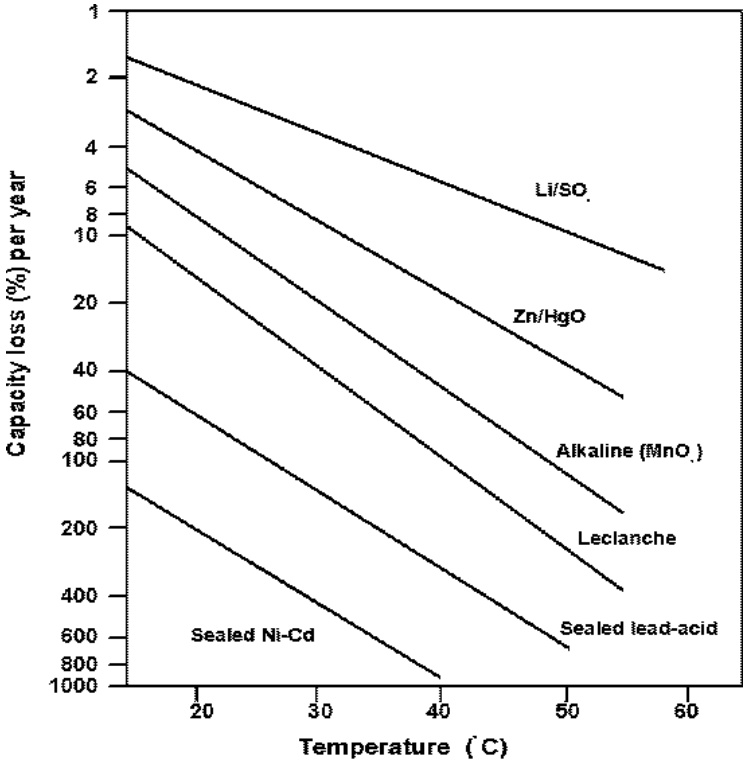

Figure 8: Self discharge capacity of different batteries with temperature (Reprinted from [9])

No requirement for priming

Most of the newly manufactured or unused rechargeable batteries do not deliver the rated capacity. They need to be formatted or primed and once this is done, they deliver the optimal capacity. Although this theory is applicable to most battery systems,

manufacturers of lithium-ion batteries disagree. It is said that Li-ion batteries are ready at right from the word go and do not need priming.

Low maintenance

Another major advantage of using lithium ion battery is that they require minimal to almost negligible repairs and maintenance to ensure that they perform at their peak level throughout their use. There is a periodic need of maintaining Ni-Cad cells to ensure that they did not exhibit the memory effect. This effect is not evident in lithium-ion batteries and thus there is no such need of maintenance.

Lightweight batteries

Lithium-ion batteries are lighter than other types of rechargeable batteries of the same size. The main reason for the lightweight of these batteries is that the electrodes of a lithium-ion battery are made of lightweight lithium and carbon.

Variety of types available

Lithium ion cells are available in different shapes and sizes for example, coin cells, pouch cells, cylindrical cells and even prismatic cell. Thus these batteries can satiate the need for almost all kinds of applications needed for different devices. A particular kind of lithium ion battery may provide a high current density and might be ideal for consumer mobile electronic equipment while another battery might provide much higher current levels and are ideal for power tools and electric vehicles.

Disadvantages

Although lithium-ion batteries have some great advantages, they also have a few serious disadvantages. Some of the disadvantages have been mentioned below [7]:

Protection required

Robustness and durability are not the strong suits of lithium-ion batteries when compared to other rechargeable batteries. Precise and accurate protection is required for them from being over charged and discharged too far. Moreover, the current must be maintained within safe limits so as to ensure safe operation. Thus, one of the major drawbacks of lithium-ion battery is that they require protection circuitry incorporated to ensure they are kept within their safe operating limits.

Ageing

Another major disadvantage of lithium-ion battery is that lithium ion batteries suffer from ageing. This is particularly harmful for those applications, which need continuously charging and discharging. This is time and calendar dependent and it is also dependent upon the number of charge discharge cycles that the battery has undergone.

Transportation

There are strict rules and regulations set for transporting lithium-ion batteries, especially by air. The batteries can be taken in aircraft carry-on luggage but special care must be taken to ensure that they are carried separately and must be protected against short circuits by protective covers, etc.

Cost

Another major disadvantage related to lithium-ion batteries are their cost. Typically the cost to manufacture lithium-ion batteries is about 40% higher as compared to Nickel cadmium cells. This might be a major issue while considering their usage in a technology or a device needing a large amount of batteries to run.

Safety concerns

Apart from previously mentioned issues, there are several ways in which lithium-ion batteries might get degraded. Therefore, extra attention must be paid and extra care and must be taken so as to avoid situations, which might lead to hazardous situations. Some of the conditions leading to such risky and dangerous situations are discussed in the section.

Voltage effects

Over-voltage

Large amounts of current flows if the charging voltage is increased beyond the recommended upper cell voltage, typically 4.2 Volts giving rise to two problems.

1. Overheating: Excessive currents may cause large increase in temperature accompanied by high amount of joule heating.
2. Lithium Plating: At high C rates and high state of charge (S.O.C) the time available for lithium ions to diffuse inside the electrodes is not enough. Thus, a large accumulation of lithium ions is formed on the surface of the anode and these ions are finally deposited as lithium metal on the surface of the anode. This is known as Lithium plating. Subsequently, this leads to an irreversible capacity loss due to

the drastic reduction in the free lithium ions. Also lithium plating is more likely to occur at low temperatures because chemical insertion of atoms into the graphite electrode becomes too slow, and Li plating becomes significant.

Lithium Cobalt Oxide and Lithium Manganese Oxide cathodes and a consequent permanent capacity loss.

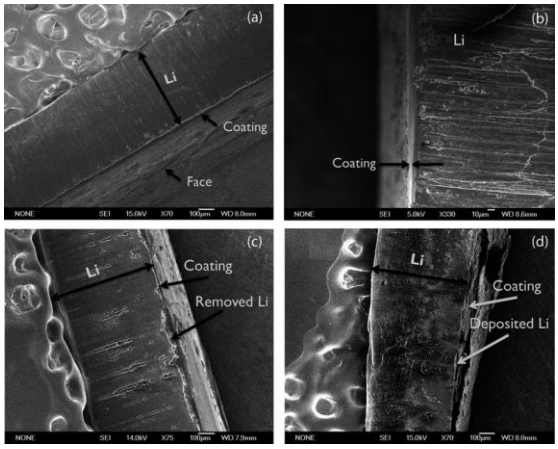

Figure 9: Lithium plating (Reprinted from [10])

A lot of research has been conducted related to this issue and it has been concluded that lithium plating is a major safety concern of Li-ion batteries because it can lead to short circuits and uncontrollably energetic chemical reactions.

Under-voltage

In situations when the cell voltage is allowed to fall below two volts lithium ion cells

suffer from the degradation by under-voltage. This usually occurs by over-discharging the cells. This results in progressive breakdown of the electrode materials. Firstly, the self-discharge rate of the cell is drastically increased because the anode copper current collector is dissolved into the electrolyte.

On increasing the voltage above 2 volts, the copper ions, which are dispersed throughout the electrolyte, are precipitated as metallic copper. These copper ions could be anywhere, and not necessarily on the current collector foil. This leads to a very dangerous situation, which can ultimately leads to a short circuit between the electrodes.

Mechanical failure

The lithium ion battery can be abused mechanically in different ways, which leads to internal short circuit, finally leading to failure. Some of the ways in which the battery might experience internal short-circuiting are crushing; nail penetration, dropping of the battery, mechanical shock to the battery, high frequency vibration and even immersion of the battery in water.

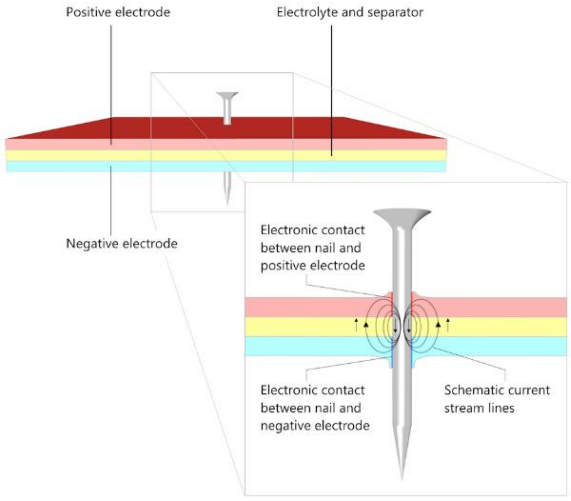

Figure 10: Mechanical degradation by nail penetration (Reprinted from [11])

Temperature effects

Temperature is known to have a significant impact on the performance, safety, and cycle lifetime of lithium-ion batteries (LiB). The battery life and capacity and is drastically impacted and the safety of the battery is compromised as the temperature reaches values above or below the normal operating range of the battery. Some of the effects of varying the temperature are discussed as follows:

Low temperature operation

The Arrhenius law states that the rate of chemical reaction decreases with decrease in temperature. The effect of this decrease in chemical reaction rate greatly affects the efficiency of the battery as all the related processes tend to slow down. The effect of reducing the operating temperature is to reduce the rate at which the active chemicals in the cell are transformed, thus the rate of the intercalation and de-intercalation of lithium

ions in the active material is drastically reduced. This might occur perhaps due to the contraction of the electrode materials due the reduced operating temperatures. This leads to an overall reduction in the rate of the electrochemical reaction, which leads to a reduction in the current carrying capacity of the cell both for charging and discharging. [12]

High temperature operation

When the cell is operated at higher temperatures than recommended, it leads to a different set of safety problems. In this case, the Arrhenius effect helps to increase the rate of the electrochemical reactions and thus in turn get higher power out of the cell. The problem with higher currents is that it gives rise to higher ohmic losses (I^2R) heat dissipation and thus even higher temperatures. These hot pockets might give rise to a situation called thermal runaway, which leads to the leads to flame and catastrophe and ultimately the failure of the battery. The next section discusses this anomaly in detail.[12]

Thermal runaway

The situation where an increase in temperature leads to situations involving even higher temperatures, often leading to a destructive result is termed as Thermal Runaway [13]. It is a kind of uncontrolled phenomenon. The dangers linked to strong exothermic reactions that are accelerated by temperature rise are the chemistry and chemical version of thermal runaway. Increased current flow in electrical engineering is analogous to the situations created during thermal runaway. Internal short circuits, physical damage, or overheating of the cell (typically from exposure to temperatures above 60°C) may trigger thermal runaway [14]. Abuse conditions (high discharge/charge rates, short circuits, and operation

at high ambient temperature) steeply accelerate the net accumulation of thermal energy in lithium-ion cells. The rate of ambient cooling increases linearly whereas the rate of heat generation increases exponentially with cell temperature, and ultimately, the cell experiences “thermal runaway” accompanied by pressure buildup, which may lead to bursting of the cell, or fire. Operation at higher temperatures decomposes the electrolyte, thus deteriorating the cell and reducing the lifetime of the cell. If the heat exceeds a critical threshold, a cathode thermal runaway situation may arise. Capacity and power reduction has also been found to occur at high operating temperature, although lowered impedance and thus increased voltage may offer better output at slightly elevated temperatures [12]. A fire or an explosion is the most common outcome of a thermal runaway.

Several stages are involved in the build up to thermal runaway and each one results in progressively more permanent damage to the cell. Stage number one of the thermal runaway involves the breakdown of the thin and protective layer of the solid electrolyte interface (S.E.I). This usually occurs due to either overheating or due to some form of physical penetration. The excessive currents, overcharging of the cell or high ambient temperature may be some of the reasons of the initial overheating of the cell. This initial overheating of the cell makes the temperature increase and once the temperature reaches about 75ºC, the SEI layer starts to break down.

When this layer gets breached the electrolyte is free to react with the carbon anode just as it did during the formation cycle but the difference being that conditions now are at a

higher temperature and more uncontrolled in nature. This takes the temperature even higher and this cycle continues in the form of an exothermic reaction.

The temperature rises continuously due to the exothermic reaction occurring as mentioned previously. As a result of this increase in heat owing to the continuous temperature rise, the organic solvents used in the electrolytes breakdown. This process usually commences at a temperature of about 100 ºC but with some electrolytes it can start at temperatures as low as 70ºC.

Due to the breakdown of the solvents dissolved in the electrolyte, there is a release of various flammable hydrocarbon gases (except oxygen) and this causes pressure to build up inside the cell. Although the temperature increases to beyond the flashpoint of the gases released by the electrolyte, the gases do not burn due to the unavailability of free oxygen.

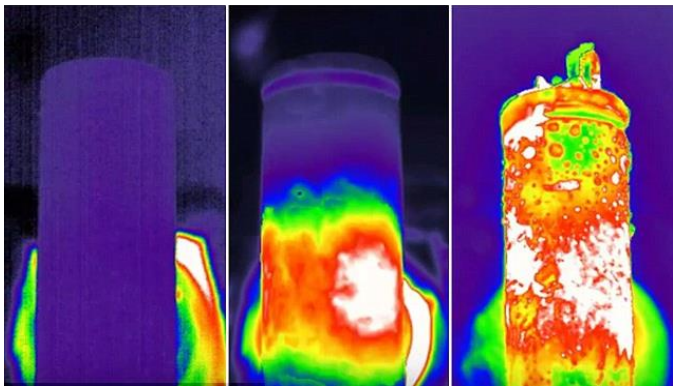

Figure 11: Thermal runaway in a cell using infrared camera (Reprinted from [15])

The cells are normally fitted with a safety vent which allows the controlled release of the gases to relieve the internal pressure in the cell avoiding the possibility of an uncontrolled rupture of the cell - otherwise known as an explosion or more euphemistically "rapid disassembly" of the cell. As a result of the safety vent, the gases are released out to the atmosphere where they can burn easily due to the availability of free oxygen.

Very high temperatures of around 135 ºC leads to the melting of the polymer separator thus allowing the short circuits between the electrodes. The heat released as a result of the electrolyte breakdown and the short circuit, causes further breakdown of the metal oxide cathode.

The breakdown of the cathode is also highly exothermic sending the temperature and pressure even higher. The cathode breakdown starts at around 200 ºC for Lithium Cobalt Oxide cells but at higher temperatures for other cathode chemistries. In most battery packs, the individual cells are small and thermal runaway in a single cell can be hazardous.

Table 1. Major hazardous incidents

Number	Date	Accidents	Location	Fire Causes
1	18th July, 2011	EV bus catches fire	China	Overheated LiFePO4 batteries
2	11th April,2011	EV taxi catches fire	China	Caused by 16Ah LiFePO4 batteries
3	3rd September,2010	A Boeing B747-400F catches fire	Dubai	Caused by overheated Li batteries
4	26th April, 2010	Acer recalled 2700 laptop batteries		Potential overheating
5	March, 2010	Two iPod Nano overheating	Japan	Caused by overheated Li batteries
6	January,2010	Two EV buses catch fire	China	Overheated LiFePO4 batteries
7	July,2009	Cargo plane catches fire before flying to USA	China	Caused by spontaneous combustion of LiB batteries
8	21st June, 2008	Laptop catches fire.	Japan	Caused by an overheated battery
9	June, 2008	Honda HEV catches fire	Japan	Caused by overheated LiFePO4 batteries
10	2006 and 2016	Thousands of mobile phones catch fire	Around the world.	Caused by short-circuit, overheating etc.

Battery thermal management system

Temperature[16] greatly affects the performance and life of batteries, so battery thermal control must be used in electric and plug-in hybrid electric vehicle under real driving conditions. In recent years, automakers and their battery suppliers have paid increased attention to battery thermal management, especially with regard to life cycle and related warranty costs. Temperature excursions and non-uniformity of the temperature inside the battery systems are the main concern and drawback for any attempt to scale-up battery cells to the larger sizes as required for high power applications. The capacity of the battery pack increases as the operating temperature is raised for a battery pack. However, this is associated with a very high expense of accelerated capacity fade. Subsequently the lifetime of the battery system is reduced.

At very low operating temperatures, the capacity available is limited and thus the performance of the battery is poor. The cycle life of a cell or a battery pack is reduced drastically if the temperature rises or falls unevenly or excessively. The reliability, lifetime, charge acceptance, power and energy efficiency are some of the factors which are affected by the non-uniformity of the temperature. Therefore, it is of utmost importance to have a uniform temperature distribution not only within one particular cell but also from one cell to another in a battery pack in order to achieve maximum cycle efficiency of the system. The battery thermal management system (BTMS) is an integral part of a battery management system (BMS) for this particular purpose. Basically, a trade-off is necessary between the cost of insulating or cooling a complex array of cells and the risk of overheating individual cells of relatively large sizes. The BTMS of a system usually

takes care of both the hardware and software in order to ensure safe and secure operation. The BTMS conducts this by making sure that the temperature difference within a cell and also between cells in a battery pack is in an optimal and safe range. Usually, the BTMS is a combination of both hardware and software to preserve the temperature difference of battery cells in a pack in an optimal range to enhance the lifetime while ensuring safe and secure operation. Simulation results showed that thermal management systems might improve battery performance by 30% – 40%. A thermal management system could be designed with a range of methods, from "simple energy balance equations" to more "sophisticated thermal and computational fluid dynamics models." Regardless of the method, the basic performance of the management system is dictated by the thermal design of each cell or module. There are two major types of thermal management systems namely: passive thermal management and active thermal management.

Passive thermal management

Passive thermal management refers to cooling technologies that rely solely on the thermodynamics of conduction, convection and radiation to complete the heat transfer process. These technologies are the most commonly used, the least expensive and the easiest to implement. The various types of passive thermal management systems are as follows:

- Heat sinks
- Heat spreaders

Active thermal management

Active thermal management refers to cooling technologies that must introduce energy typically from an external device to augment the heat transfer process. A key benefit is

that they increase the rate of fluid flow during convection which dramatically increases the rate of heat removal. Their drawbacks include the need to use electricity in order to operate, the possible introduction of audible noise to a system, and the fact that they are generally more complex and expensive than passive systems. The types of Active thermal management systems are as follows:

- Forced Air
- Forced Liquid
- Solid state heat pumps

The following two figures show the thermal management techniques used by the two major automobile manufacturers namely Tesla and General Motors. Most of the cars automobiles employ the Active or the Forced thermal management technique mainly due to its higher efficiency in the heat removal process. The Tesla's thermal management system uses liquid Glycol as a coolant. This coolant is made to travel through all the cells in the module in order to absorb the heat. The thermal management system employed in the Tesla transfers the heat absorbed by the coolant to a refrigeration cycle and use electric resistance heating in cold weather.

On the other hand, General Motors uses prismatic or rectangular shaped lithium-ion cells. The size of the cell is larger than the usually employed cells in electric vehicles and hybrid electric vehicles and is roughly the size of a children's book. A cooling aluminum plate is sandwiched between the cells. There are 5 individual coolant paths passing thru the plate in parallel not in series as the Tesla system does. Each battery pouch (cell) is housed in a

plastic “frame” The frames with coolant plates are then stacked longitudinally to make the entire pack.

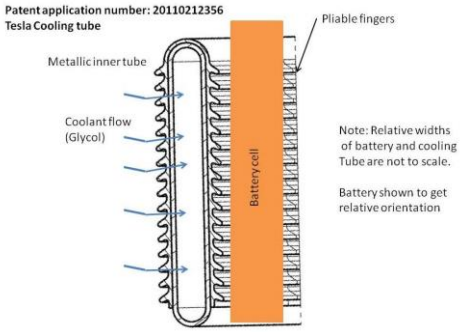

Figure 12: Thermal management system used in Tesla vehicles

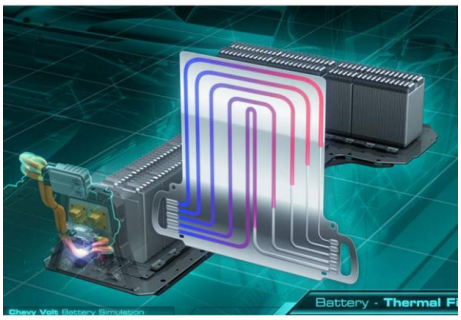

Figure 13: Thermal management system used in General Motors vehicles

CHAPTER II

LITERATURE REVIEW

The electrical and electrochemical phenomena in a Li-ion cell have been widely studied but relatively lesser literature exists on thermal transport in a Li-ion cell[17]. The electrolyte, at temperatures higher than critical temperatures, gets decomposed, releases and catches fire and ultimately a cathode thermal runaway situation may arise. Thus, this degrades the cell performance and in turn reduces its lifetime Capacity reduction and power reduction has also been found to occur at high operating temperature.

A typical lithium-ion cylindrical cell is made up of a composite layered material, which consists of the anode; the cathode, the separators and the current collectors soaked in electrolyte and rolled in a Swiss roll fashion. Electrode tabs are present at the ends of the cell to collect the electric current and then to conduct this electric current to the external cell terminals. The nature of the axial thermal transport is significantly different from the radial thermal transport as a result of this construction of the cell. This specific construction of the lithium ion 18650 cell leads to a drastic difference in the transport properties such as heat capacity and thermal conductivity in both the radial and the axial direction. In the axial direction, due to the absence of different contact resistances, thermal conduction is expected to occur primarily along the current collector materials, which often run continuously in the axial direction. On the other hand, in the radial direction, there are multiple contact resistances between the different materials of the jellyroll as a result of which the heat flow in the radial direction is impeded drastically and thus the

overall value of the thermal conductivity is significantly different in both the directions. Significant thermal resistance is presented as a result of the thermal contact resistance preset between different materials inside the cell, sometimes even greater than the material thermal resistance itself. It is of utmost importance to address this issue of anisotropy present in the cells due to the variations in the thermal properties as a result of its construction. It is paramount to experimentally measure the radial and axial thermal conductivities of a cylindrical Li-ion cell because the assumption of isotropic thermal transport properties in Li-ion cells design would lead us to either under predict the value or over predict the value of the temperature field both of which would lead to highly undesirable results.

Zhang et al.[18] investigated the heat generated inside a cylindrical lithium-ion battery consisting of graphite as the anode, LiPF6 as the as the electrolyte and spinal as the cathode. The electrolyte transport properties as functions of temperature and Li ion concentration are considered while developing the coupled electrochemical-thermal model. The different sources of heat generation namely the reaction heat; the ohmic heat and the active polarization heat are quantitatively analyzed for the battery discharge process. The thermal conductivity depends on the temperature and the concentration and is given as follows: $k= 1 \times 10^{-4}c\ (-10.5 + 0.074T - 6.69 \times 10^{-5}T^2 + 6.68 \times 10^{-4}c - 1.78 \times 10^{-5}cT + 2.8 \times 10^{-8}cT^2 + 4.94 \times 10^{-7}c^2 - 8.86 \times 10^{-10}c^2T)^2$ It is concluded that the ohmic heat is the largest contributor of heat generation with around 54% of the total heat generation. About 30% of the total heat generation in average is ascribed to the

electrochemical reaction. The active polarization is the smallest contributor as compared to the ohmic heat and reactions heat. The main factors giving the effect on the heat generations of active polarization and electrolyte electric resistance are lithium-ion concentration and its gradient in the electrolyte.

Chen et al. [19] carried out the thermal analysis of lithium-ion batteries during charge/discharge and an analysis to study the thermal runaway with a mathematical model. The main concern, which was addressed in this study, was the thermal behavior of batteries in a scenario of a sudden and significant temperature increase, which might lead to a thermal runaway situation. The examination of the battery design parameters and operating conditions on temperature rise/profile during normal battery operation and the valuation of the possibility of the occurrence of thermal runaway due to battery abuse is greatly emphasized in this work. The thermo-physical properties like thermal conductivity and heat capacity were taken from reference papers or optimal values were chosen. It was observed that during normal battery operation, the battery temperature did not reach the temperatures needed to initiate the thermal runaway although heat may not be dissipated out of a large cell stack during high rate discharge. But if the cell is cycled at very high C-rates during both charge and discharge, there is significant amount of heat accumulated in the cell and the temperature reached in this situation is high enough to lead to the thermal runaway situation after which the temperature rises continuously.

The following table gives the selected values:

Table 2. Thermal properties of different materials

Material	Heat Capacity (J/ g K)	Thermal Conductivity (W/m K)
Copper	0.385	398
Aluminum	0.900	237.0
Negative Electrode	1.184	1.400
Separator	2.066	0.83
Positive Electrode	1.134	2.18

T. D. Hatchard, et al. [20] developed a predictive model for oven exposure testing by using reaction kinetics that have been developed for electrode materials with electrolyte exposed to high temperatures , and thermal properties of cells from the literature. The model predictions were shown to be in excellent accord when compared to oven exposure test results for 18650 LiCoO2/graphite cells. For the development of the mathematical model, the values of average heat capacity and average thermal conductivity of different components of the cell were taken from literature[21]. The model, without the production of actual cells was able to predict the response of new cell sizes and electrodes. This was demonstrated with a few examples such as the model was able to predict the changes while using LiMn2O4 or other cathode substitutes instead of LiCoO. Moreover it could also predict how increasing the specific surface area of the graphite electrode would have an

impact on its performance. The model was also able to predict the changes that would be seen while varying the thickness of prismatic cells or varying the diameter of cylindrical cells without the need to produce actual cells. Noboru Sato et al.[22] carried out thermodynamics experiments and studies for the lithium-ion Li-ion batteries that are used as the power sources for electric and hybrid vehicles. The charging and discharging of the cell has a huge impact on the amount of heat coming in and going out, respectively. The different factors, which lead to heat generation in the cell, are as follows: reaction heat value Q_r, polarization heat value Q_p, and Joule heat value Q_J. Moreover, the degree of contribution of each factor could be expressed quantitatively by dividing these thermal generation factors for charging and discharging. The thermodynamics calculation coincided with the experimental data of thermal generation for the practical Li-ion batteries for electric vehicles EV and thus the accuracy of the thermodynamic logic was verified. It was concluded that the values of each of the contributors to the heat generation is as follows:

Reaction heat $Q_R = 3.73 * 10^{-2}\ Q1 * I$

Polarization heat Qp = $3.60 * R_p * I^2$

Joule heat $Q_J = 3.60 * R_c * I^2$.

Carolyn R. Pals et al.[23] presented two different models to predict the thermal behavior of the lithium/polymer battery. The first part of paper presents the one-cell model, which is a one-dimensional model for predicting the thermal behavior of the lithium negative electrode/solid polymer separator/insertion positive electrode cell. The cell-stack model, which is a one-dimensional model that uses variable heat-generation rates calculated by

the one-cell model to predict temperature profiles in cell stacks, is presented in the second part of the paper. The one-cell model, presented in the first part, is based on the model of Doyle et al [24] with the addition of an energy balance in the form given by Bernardi et al [25]. The physical properties are allowed to vary with temperature. With increasing temperature, the cell potential, along the active material utilization at the cutoff potential increases. Moreover with increasing temperature, it was seen that the heat generation rate of the cell decreases. Cells operating isothermally above $90^o\ C$ are ohmically limited. In adiabatic discharge, a local minimum in cell potential is observed for currents above 2.0 mA/cm^2, and above 4.0 mA/cm^2 the melting temperature of lithium is reached.

S. Al Hallaj et al. [26] worked on simulating temperature profiles inside lithium-ion cells by developing a simplified one-dimensional thermal mathematical model with lumped parameters. The model uses the Sony 18650 cell in order to use parameters of heat-generation. The simulations did show some deviations from the temperature measurements at C/1, but at C/2, C/3, and C/6 discharge rates, the simulation results showed good agreement with temperature measurements. The model was used to simulate temperature profiles under different operating conditions and cooling rates for scaled-up cylindrical lithium-ion cells of 10Ah and 100 Ah capacities. Results showed a strong effect of the cooling rate on cell temperature for all discharge rates. A significant temperature gradient inside the cell was found only at higher cooling rates, where the Biot number is expected to be more than 0.1. At lower cooling rates, the cell behaves as a lumped system with uniform temperature.

Salvio Chacko et al. [27] with a view to develop an effective battery thermal management system, modeled the time-dependent, thermal behavior of a lithium-ion (Li-ion) polymer for electric vehicle (EV) drive cycles The developed model is based on the finite volume method and is a fully coupled, three-dimensional transient electro-thermal model. Various tests were conducted under different loading cycles consisting of various charge-discharge rates, for a high energy density lithium-ion pouch cell. A good agreement was found between the model predictions and the experimental data. The cell- level thermal behavior was tested under two different conditions: mild operating conditions and severe operating conditions. For mild accelerations, the temperature of the cell was found to remain in the optimal range and thus the requirement for a thermal management system was not important. Incase of severe operations, i.e. in case of under stressful conditions such as high power draw during rapid and high accelerations and decelerations, a significant temperature increase was observed thus indicating that an effective battery thermal management system would be required to maintain the optimal cell performance and also to achieve a full battery lifespan.

L.H. Saw et al. [28] developed a pseudo two dimensional electrochemical model which is coupled with the lumped thermal model in order to analyze the electrochemical and thermal behavior of the commercial 18650 Lithium Iron Phosphate battery. The dimensions of the current collector, separators, casing thickness, electrodes, and the gasket was obtained by cutting the cell. The layer structure of the spiral wound, cylindrical casing, gasket and heat shrink-wrapping were modeled The temperature distribution across the cell was better understood by modeling the layer structure of the spiral wound, cylindrical

casing, gasket and the heat shrink-wrapping. Natural convection and radiation were used to reflect the heat dissipation on the side surface. Experiments were performed in order to compare and verify the simulation results. The simulation results suggested that the cell temperature and total heat generation rate have a positive correlation with the C-rates and these were inline with the experimental results. It was observed that the reaction heat contributed about 80– 85% to the total heat generated and was the major contributor of heat during charging and discharging of the cell. An investigation of the electrical contact resistance between the connectors and terminals of the cell was also performed and it was found that the electrical contact resistance caused a large temperature gradient across the cell. These effects suggest that an efficient battery thermal management system is necessary in order to avoid the extreme conditions in the cell, which might lead to thermal runaway.

Akram Eddahech et al. [29] focuses the research on the thermal behavior of high-power lithium-ion cells during charge-discharge at different current rates. In order to promote an adiabatic environment during testing, the accelerating rate calorimeter is for all the tests. Cell entropy is measured, using both potentiometric and calorimetric methods. Basically, the internal resistance to current flow leads to the joule heating effect, while the electrochemical reactions that occur during charge and discharge modify battery entropy, thus affecting heat generation. Entropy was measured using both potentiometric and calorimetric methods, in order to quantify the reversible heat component and the results confirmed its significant dependence on SOC variations. At higher C-rates, the impact of

the change in entropy on the heat generation is significantly less, which implies that at higher C rates, during charging and discharging, the irreversible heat component is much larger.

In all the previously cited research papers, the heat generated inside of a lithium-ion cell has been thoroughly studied and different contributors to the heat generation have been identified. It can be concluded from almost all the research papers that main contributor of heat generation inside a lithium-ion cell is the ohmic heat or the irreversible heat. The heat of reaction is the next major contributor to the heat generation in the cell. The point to be highlighted is that to calculate the heat generated in the cell and to find out the various contributors of heat, it is essential to know the precise values of the thermo-physical properties of the cell such as the heat capacity and the thermal conductivity. The accuracy of any heat generation model rests on the fact that values of the thermos-physical properties used are error-free and correct. In all of the previously discussed papers, the heat generation has been calculated using inaccurate and flawed values for thermal conductivity and heat capacity of a lithium-ion battery. In most of the research conducted to determine the heat generated inside the battery, the average values of the heat capacity and the isotropic values for the thermal conductivity have been used. These isotropic values of thermal conductivity are highly incorrect and have a very large error when compared to the actual values in each direction or the anisotropic values. As discussed previously, the contact resistance offered in the radial direction is much larger as compared to that in the axial direction due to the internal structure of the lithium-ion cell. Thus, the

thermal conductivity is expected to be much smaller in the radial direction when compared to thermal conductivity in the axial direction. Assuming a constant value in both the direction leads to the large erroneous values of heat produced inside the cell. If the value of k_r (radial thermal conductivity) is used as the thermal conductivity of the entire cell, then we would be using a severely lower value of conductivity for the axial direction, since the actual conductivity in this direction is at least hundred times greater than that in the radial direction. Moreover, if we use k_z (axial thermal conductivity) as the conductivity of the entire cell, then we would be using a tremendously high value of conductivity for the radial direction which would again lead to erroneous value of heat generated inside the cell. Thus, it is of utmost importance to experimentally calculate the values of the heat capacity and the thermal conductivity of the cell in each direction which would help us better understand the heat generated within the cell and thus help us design more efficient thermal management systems in order to counter-attack this heat generated.

Heinrich et al [30] [31, 32] uses a modified steady state technique which uses two heat flux sensors instead of one. This method is also referred to as flux deconvolution technique. The parameter (conductivity, heat capacity) estimation is achieved through the deconvolution of these signals and the identification of the system impulse response. A detailed derivation of the theoretically expected behavior has been done, which provides a basis for fitting the measured impulse response. A six term expansion is required for the theoretical model to achieve full convergence. The parameter estimates of the standard test samples are excellent, with average errors of 2.3% for brass and 6.3% for aluminum.

The system has several advantages in addition to the short measurement time, including low cost and no guard furnace or insulation requirement for room temperature measurements. The main disadvantage is that the signals are very noisy due to the frequency domain division required by the deconvolution. Also, the fitted values of thermal conductivity are having a large error when compared to experimental data [33].

B E Belkerk et al [34] [35] [36] used the ultra-fast transient hot-strip (THS) technique for determining the thermal conductivity of thin films and coatings of materials on substrates. Precise measurement of thermal conductivity was performed with an experimental device generating ultra-short electrical pulses, and subsequent temperature increases were electrically measured on nanosecond and microsecond time scales. The thermal conductivity of the films was extracted from the time-dependent thermal impedance of the samples derived from a three-dimensional heat diffusion model.[37]

S.J. Drake et al [17] [38] used the unsteady adiabatic heating technique experimental technique to measure the anisotropic thermal conductivity and heat capacity of Li-ion cells. Experimental measurements indicate that radial thermal conductivity is two orders of magnitude lower than axial thermal conductivity for cylindrical 26650 and 18650 LiFePO4 cells [39] . The major disadvantage of the technique is that the entire experiment needs to be performed inside a vacuum chamber so as to neglect the losses due to convection and radiation which is one of the underlining assumptions of the experiment [40].

An Cai et al [41] a laser flash technique to carry out measurements of thermal diffusivity of layered anodic aluminum specimen, while the effective thermal conductivity of anodic alumina film was determined using a two-layered model. The results showed that the thermal conductivity of anodic alumina films has a temperature dependence of amorphous solids, and the apparent thickness dependence of thermal conductivity is not found for anodic alumina films. The major disadvantage of this technique is that the laser flash method is only applicable to suitably thin discs or films as stipulated by the ISO standard 22007-4:2008. Also, for some composites such as foams which are very brittle, it is difficult to obtain very thin slices.

Evgenij Barsoukov et al [42] introduced novel characterization of thermal properties of batteries by defining their frequency dependent thermal impedance functions. The thermal impedance function can be approximated as a thermal impedance spectrum by analyzing the experimental temperature transient which is related to the thermal impedance function through the Laplace Transform. Comparison of the spectra at different states of charge indicates an independence of thermal impedance on the SOC. Also, it is shown that the thermal impedance spectra can be used to obtain simultaneously the heat capacity and thermal conductivity of the battery by nonlinear complex least squares fit of the spectrum to the thermal impedance model.

Matthias Fleckenstein et al [43] introduce a new approach of Thermal Impedance Spectroscopy (TIS) for thermal characterization of battery cells. It examines the transfer

behavior between internal heat generation and resulting battery surface temperature in the frequency domain. The complete procedure is demonstrated by the TIS-application on a cylindrical High-Power Li-Ion cell. By the use of a thermal battery model, its theoretical transfer function can be fitted to the TIS-measurement results in the Nyquist-Plot. Consequently, the specific heat capacity and the heat conductivity of the cell's jelly roll can be derived. Compared to conventional thermal characterization methods the TIS showed good agreement of results for the specific heat capacity. A possible explanation for the relative difference of 12% in the thermal conductivity determination given was that the measurement conditions that were closer to real life operation for the TIS method. Consequently, a main portion of the deviation could be attributed to the difference of the heat conductivity of a deep discharged jelly roll (as investigated in the conventional method) and the jelly roll in a regular operation range (as investigated in the TIS). Following, there are indication that the inaccuracy of the exemplary operated TIS is even less than 12%.

Krishna Shah et al [44] present a review paper which presents a critical analysis of recent research literature related to experimental measurement of multiscale thermal transport in Li-ion cells. Recent research on several topics related to thermal transport is summarized, including temperature and thermal property measurements, heat generation measurements, thermal management, and thermal runaway measurements on Li-ion materials, cells, and battery packs. Key measurement techniques and challenges in each

of these fields are discussed. Critical directions for future research in these fields are identified.

CHAPTER III

PROPOSED TECHNIQUES

Proposed experimental setup

The main objective of this research is to develop a feasible, economical as well as a non-invasive technique to determine the heat capacity and anisotropic thermal conductivity of any given cylindrical body with a specific set of dimensions. There have been quite a few techniques discussed in the previous chapter to deduce these thermo-physical properties but there are some major problems and issues associated with them such as the practicability of the entire setup, the cost factor of the expensive equipment used as well as the limited applicability of the technique to a very specific set of materials. So, the main motivation to conduct this research was to acquire these thermo-physical properties using a novel, non-invasive and most importantly a realizable technique. The dimensions of this test body should be similar to that of an 18650 lithium-ion battery. The height should be fixed to 65mm and the diameter of the block should be around 18mm. Since the purpose of the experiment is to develop a non-troublesome as well as an economical technique, the experimental setup consists of a limited number of small components. All the materials and components needed to build the entire setup are easily available in the market. Moreover, the highlight about this work is that the entire setup can be constructed within a span of four days in a simple mechanical workshop, which really makes it feasible and elementary to create, by anyone. The experimental setup consists of a just 4 main components namely a wooden block, a thin aluminum sheet, a heating coil, thermocouples and an Arbin system to power the experiment. Each component including its material and

type was chosen after intense brainstorming and after coming up with a fair and logical explanation and justification.

So firstly, there was a need to find a material to make up the base of the setup. For this purpose, we needed a material having high thermal resistance and very low thermal conductivity. The main idea was to avoid as much heat loss as possible from the setup and to keep the system almost adiabatic in nature. Most of the metals have a very high thermal conductivity and thus they could not be used for this purpose. Moreover, the non-metallic materials like plastic and Styrofoam although have a very low thermal conductivity but could not be used because of their low melting point as well as low yield strength and thus using them would have made the entire setup less robust which again defeated the purpose of the research. Wood as a material is not only robust but also has a very low thermal conductivity and thus it was used to make the base of the setup. Wood is a natural insulator due to air pockets within its cellular structure, which means that it is 15 times better than masonry, 400 times better than steel, and 1,770 times better than aluminum. The ideal insulator for energy is a vacuum, or space that is completely empty, because the absence of molecules means that no vibrations are taking place. Vibrations at the molecular level build heat energy. While wood appears solid, it is a highly porous material, and there are internal crevices within wood that store heat readily. Another great advantage of using wood is that it is easily machinable and thus making the setup with precision was achieved with no additional challenges.

The following images show the step-by-step development of the wooden set. The right side images show the solid works model of the real life images presented on the left hand side.

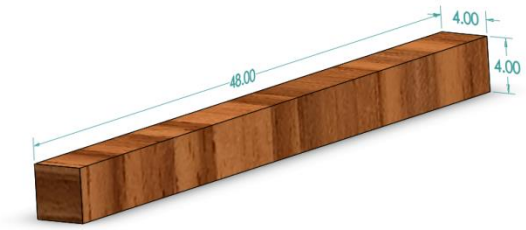

Figure 14 : Original piece of wood

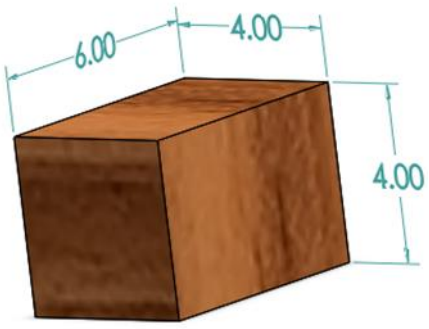

Figure 15: Machined piece of wood used for the actual setup

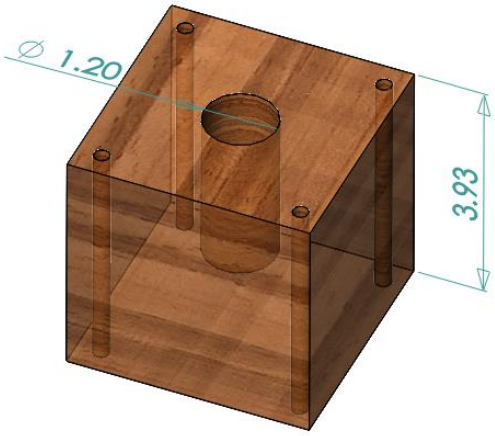

Figure 16: Bottom part of the assembly

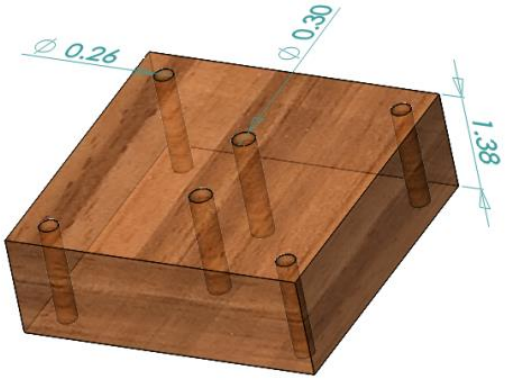

Figure 17: Top part of the assembly

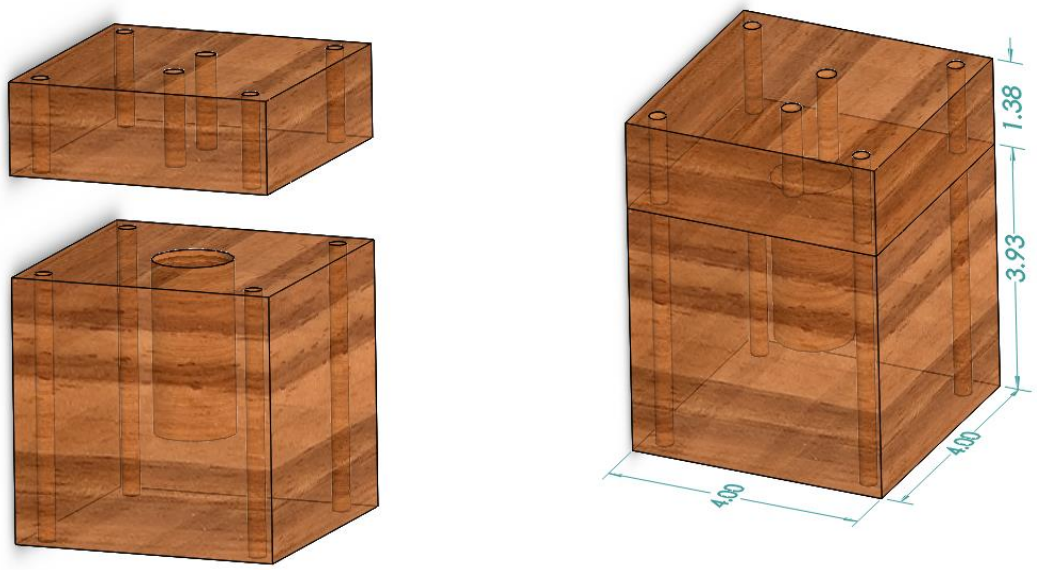

Figure 18: Complete assembly and its exploded view

The next step was to decide the device, which would be used to measure the temperature response of the test block being heated. For this purpose, we needed a device, which was not only accurate and flexible but also small so that it could easily fit inside the wooden setup. The devices, which were looked into, were thermistors, resistance temperature detectors, thermocouples and lastly pyrometers. Thermocouples were an obvious choice for this operation because the other devices were either quite expensive or quite rigid and big to fit inside the setup created. Thermocouples are the most simple, rugged, strong and the most economical temperature sensors which are used in a wide variety of applications [45]. A thermocouple is made up two wires of dissimilar metals and these wires are joined at one end [46]. When these two wires made up of dissimilar metals are joined at both

ends and one of the ends is heated, there is a continuous current, which flows, in the thermoelectric circuit [45] [46].

Figure 19: Thermocouple

This means that when the junction of the two metals is heated, or cooled, a voltage is produced that can be correlated back to the temperature. When properly configured, thermocouples can provide measurements over a wide range of temperatures. Thermocouples are known for their versatility as temperature sensors and thus thermocouples are manufactured in a variety of styles, such as thermocouple probes, thermocouple probes with connectors, transition joint thermocouple probes, infrared thermocouples, bare wire thermocouple or even just thermocouple wire.

Thermocouples are available in different combinations of metals or calibrations. The most common are the “Base Metal” thermocouples known as Types J, K, T, E and N. There are also high temperature calibrations – also known as Noble Metal thermocouples - Types R, S, C and GB.

Table 3. Different Thermocouples [45]

Common Thermocouple Temperature Ranges			
Calibration	**Temperature Range**	**Standard Limits of Error**	**Special Limits of Error**
J	0° to 750°C (32° to 1382°F)	Greater of 2.2°C or 0.75%	Greater of 1.1°C or 0.4%
K	-200° to 1250°C (-328° to 2282°F)	Greater of 2.2°C or 0.75%	Greater of 1.1°C or 0.4%
E	-200° to 900°C (-328° to 1652°F)	Greater of 1.7°C or 0.5%	Greater of 1.0°C or 0.4%
T	-250° to 350°C (-328° to 662°F)	Greater of 1.0°C or 0.75%	Greater of 0.5°C or 0.4%

For our research, thermocouples of type K were selected simply due the facts that not only were they economical, but also small in size with high precision which were important factors to the experimental setup.

The next component selected was a rope heater also called a heating coil. This component was again mainly selected due to its property to be flexible. The internal structure of the flexible rope-type heating element is made up of a high temperature proof material, which is further wound up, in a resistant yarn. This yarn is further insulated to improve the efficiency of the heating rope [47]. These ropes operate by utilizing a proprietary method of wire winding which thus helps them to offer a very high watt density as compared to other heating elements available in the market. [47]The main features and advantages of using the rope heater are that they are the most economical method of heating the test block used. Also, they are available in a wide range of wattages and thus this extends their scope of usage. The heating coil used in our research is the OMEGALUX rope heater.

Figure 20: Omegalux heating coil

Tubes with diameters as small as 1/8" (3.2 mm) can be heated by using these rope heaters as the heating element [48]. A 24" (610 mm) long fiberglass insulated lead wire is at the end of each rope heater. The specifications are as follows [48]:

- Maximum Allowable Temperature: 482°C (900°F)
- Suitable for Use on Conductive Surface: Yes
- Resists Moisture, Vapor, Or Chemicals: No
- Standard Diameter: 5 mm (3/16 inch)
- Voltage: 120 Volt ac or dc, 240V optional
- Linear Wattage: 4 Watts/in. approx.
- Heater Length: 3, 6, 8, or 10 feet (0.9, 1.8, 2.4 or 3.0 m)
- Lead Length: 24 inches (609 mm)
- Termination: Stripped leads

The next equipment required is to provide the heat flux to the test block inside the setup. For this purpose, the Arbin systems are used. The Arbin Instruments' BT2000 is a multiple independent-channel testing system mostly used for the lithium-ion batteries characterization in MSAL. The system has system has 20 channels for 20 different cells and 16 auxiliary channels for temperature measurements. Each channel operates independently of the others enabling users to run tests on multiple batteries at the same time. Each channel in the BT2000 is a true potentiostat and galvanostat with charging and/or discharging capability. Electrochemical test experimental procedure is defined by

user in the “schedule” file. Each schedule is a combination of sequential steps that define: (1) a controlling tests function and its value; (2) the termination conditions for each step; (3) the next step that the testing is scheduled to go to when the present step is finished; (4) data logging criteria. Each schedule is stored in the file with an extension of *.sdu. Each schedule may consist of as many steps as desired. Once the test schedules are defined, each schedule can then be assigned to any channel during creating a test batch. The schedules are stored in the MITS Pro Files/Schedule Files directory. The schedule/ protocol used in the our research was a three step one and is shown as follows:

1. Initial Rest (0.5 hour)
2. Power (Current applied for a preset time)
3. Final Rest (6 hours)

The screenshot of the actual protocol in the Arbin system is also shown as follows:

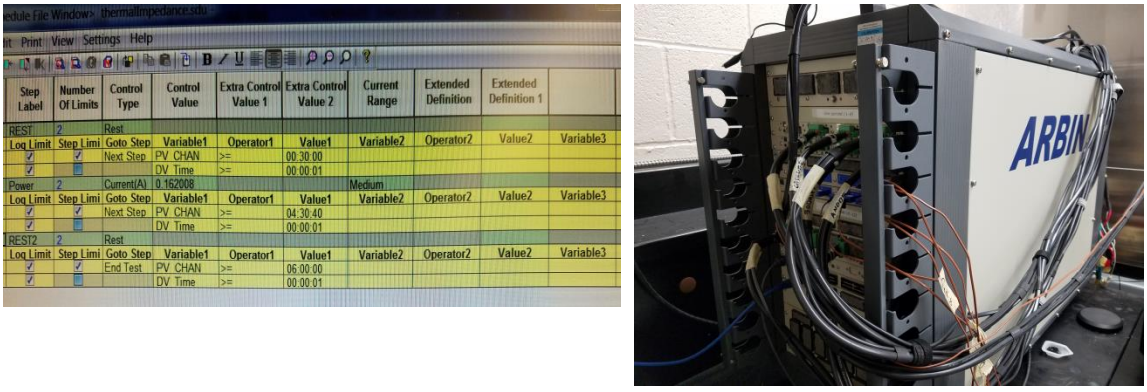

Figure 21: Protocol used for the tests and the Arbin system

Problems encountered with the experimental setup

Once the setup was completely developed and the theoretical and computational groundwork was laid, it is absolutely necessary to test the setup in order to make sure that the setup actually works and can help us achieve our goal. The objective of the preliminary experiments performed is to justify that the setup developed is perfectly suited to the tests and measurements, which need to be performed. The setup can be proved flawless only by making sure that the setup is completely insulating with no or negligible heat loss. This was not only necessary for the better results, but also to the technique developed. Any amount of heat loss from the setup would render the theoretical technique useless giving us junk values. The following points were thoroughly studied and subsequently justified.

Firstly, it is to be made sure that the heating coil length is such that it wraps only around the desired surface of the testing block. This ensures that the entire heat provided by Arbin system to the heating coil is transferred to the desired parts of the testing block only and all other areas remain adiabatically insulating. It was made sure by visual inspection that the heating coiled wrapped around the testing block completely with no extra length of the coil going unused or wasted. The radial setup was tested and the heating coil was wrapped only on the radial part of the aluminum block with the two end surfaces of the cylinder completely insulated inside the experimental setup.

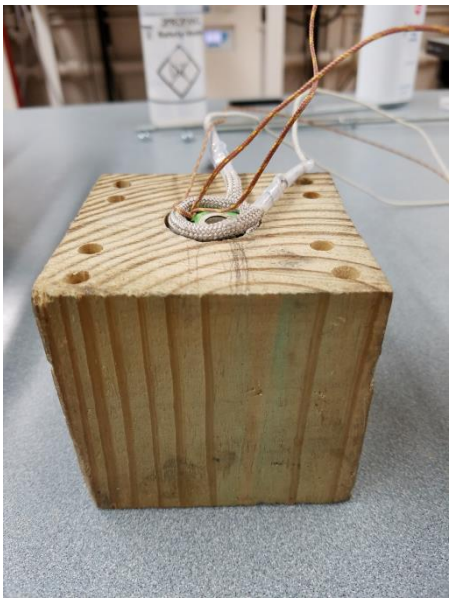

Figure 22: Block with thermocouples wrapped around with heating coil

The second point, which was studied, was that of distribution of the provided heat. It is of utmost importance that the heat being provided by the heating coil to the testing block in the form of current should be uniformly distributed to the entire block without having any kind of thermal hotspots. Using an extremely thin aluminum sheet and wrapping it around the testing block before wrapping it with the heating coil resolved this issue. This ensured that all the heat provided by the Arbin system was reaching every part of the block uniformly with no hotspots. The below image shows the thin aluminum casing used in all the experiments performed.

Figure 23: Aluminum casing

The next point, which was investigated, was of uniformity of the thermocouple readings. In some of the results, the thermocouples were showing different temperatures at the same time and were highly inconsistent. This could either occur due to the non-uniformity in the manner of the placement of the heating coil or due the lack of calibration of the thermocouples. As discussed in the previous point, the position of the heating coil w.r.t. the setup and the test block was fixed and thus the heat provided is uniform and equal in all directions. Thus, all the thermocouples were calibrated in order to reduce the variation in the temperature recorded at a single time by the system. A **multi-point calibration** test was performed where the thermocouples were placed in a thermal chamber. The temperature of the thermal chamber was set to different values and the corresponding temperature response of the thermocouples was recorded in the system. The following steps were performed for the calibration:

1. The mean temperature of the chamber and the mean temperature of each of the thermocouple was calculated.
2. Using these average values, a linear curve fitting was performed and a tread line was obtained for each thermocouple and the chamber.
3. The values of the temperature recorded in the Arbin system for the thermocouples was used to find the corresponding X coordinate using the equation of the tread line obtained.

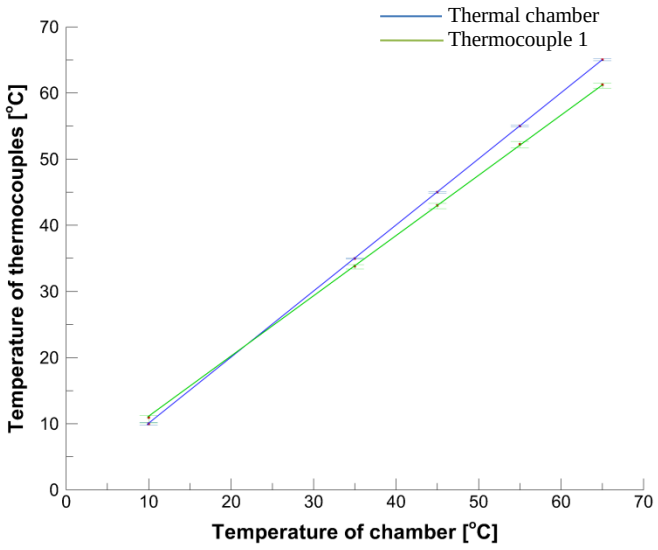

Figure 24: Curve fitting

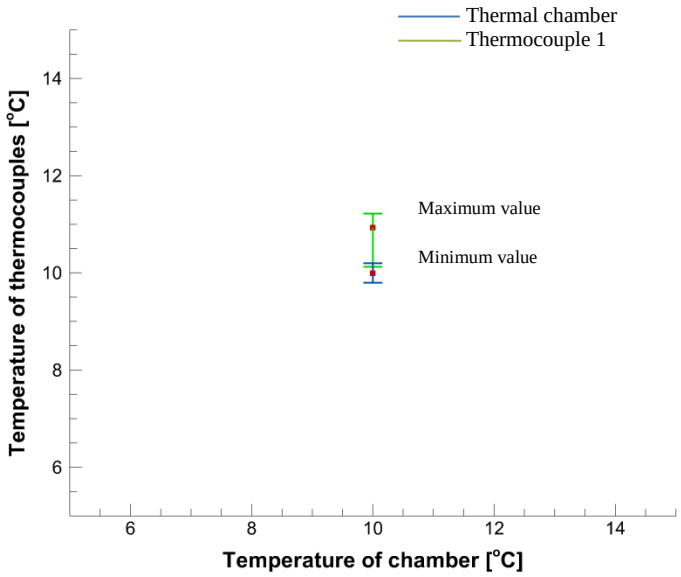

Figure 25: Zoomed view of error bat at T = 10℃

4. Now substituting this X coordinate value in the equation of the tread line obtained for the thermal chamber gave us the corrected or modified temperature value for the thermocouples.
5. The same procedure was repeated for all the thermocouples used in the experiments and the modified data was recorded.

The next set of experiments were performed on an 18650 lithium-ion cell. This set of experiments was performed to test the insulation of the developed experimental setup. Two different sets of experiments were performed. The power was increased from two watts to three watts to check if a higher temperature was achieved using a higher power

rate. In each step, an extra layer of insulation was added and the test was run. The first layer of insulation added was a bubble wrap paper. This was used to wrap the entire external surface of the setup. Bubble wrap was mainly used because it is a really good insulating material and also really economical and thus it serves the purpose perfectly. The second step of insulation used was a cardboard box. The box was used to cover the entire setup and additional holes were made in order to accommodate the heating coil and thermocouple wires. Additionally, molten wax was used to fill in any holes in order to avoid any loss of heat through them. No additional changes were made to the experimental setup. The same protocol was used for all the experiments.

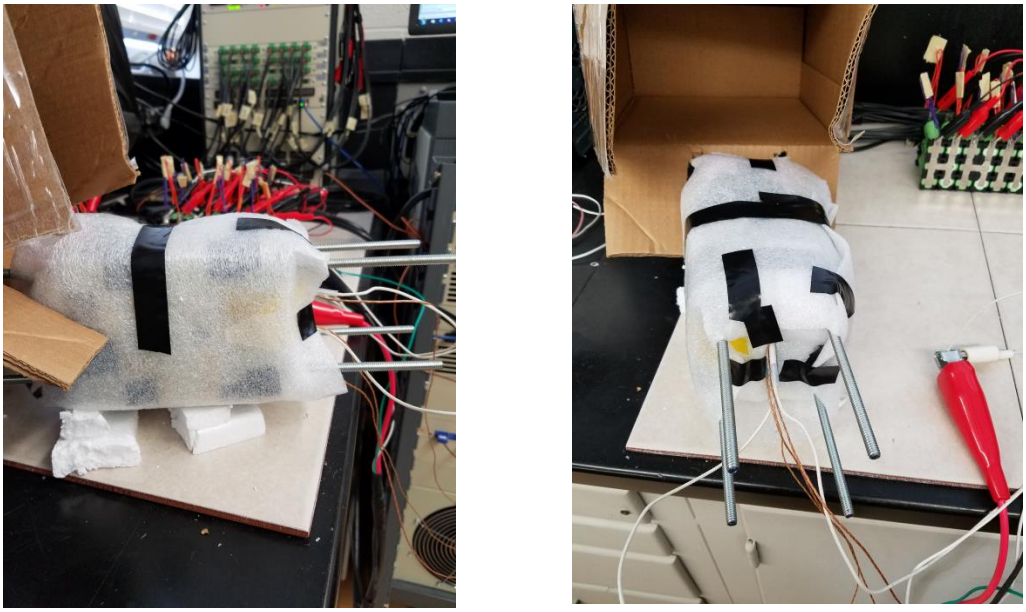

Figure 26: Setup insulated with bubble wrap

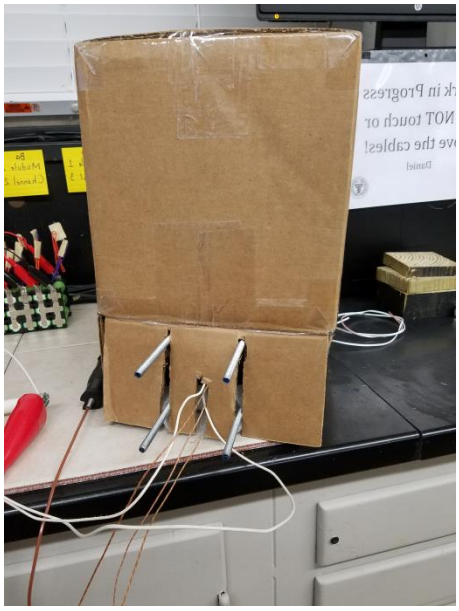

Figure 27: Setup insulated with bubble wrap and cardboard box

Tests

Test 1

In this experiment, the tests were performed using the same power of 2W but different stages of insulation. In these experiments, the first test was performed using no insulation and the test was run until it reached a quasi-equilibrium state. These experiments were performed to have a benchmark for the next set of experiments, which were performed using some kind of insulation. The following graphs show all the details clearly.

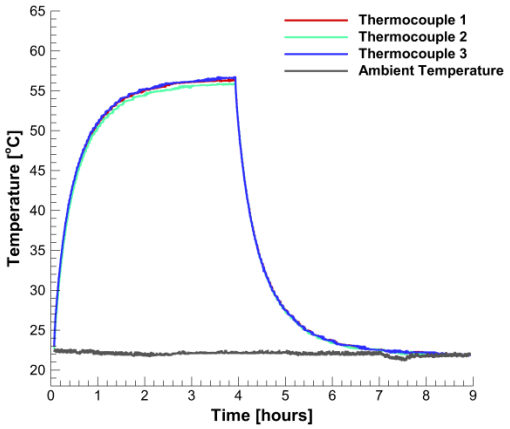

Figure 28: No insulation

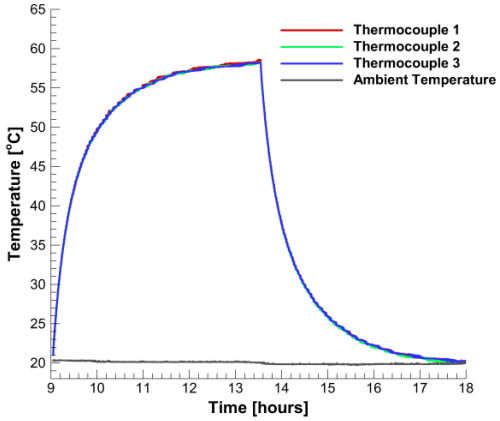

Figure 29: Modified setup

As expected, the bubble-wrap helped improve the insulation of the setup. This is visible from the graphs. The thermocouples reach a higher temperature when the test was run using the bubble wrap insulation. The temperature increased by about $2.5^{o}\ C$. We also see the expected linear profile more clearly after a few hours of testing. This shows that the bubble wrap improved the insulation of the setup.

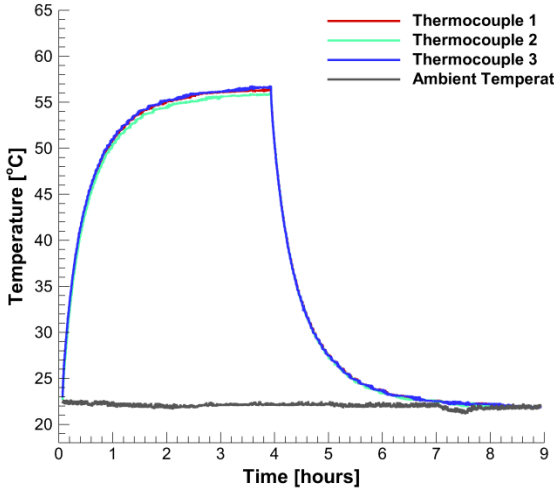

Figure 30: Unmodified setup

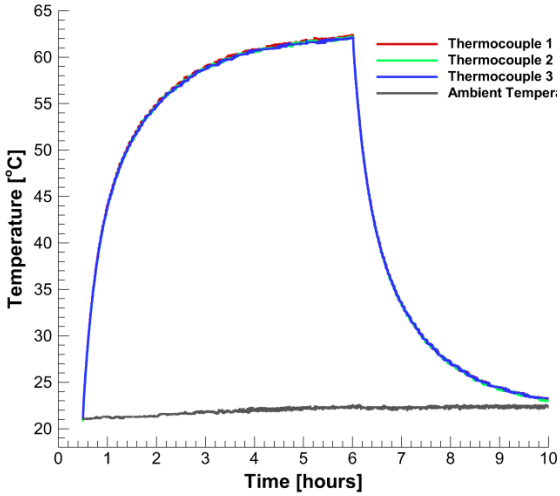

Figure 31: After added paddings to insulate setup

After the first test, the insulation was further tried to improve by adding an insulating cardboard box over the setup. The graphs show that the insulation further improved as an even higher temperature was achieved with the additional box. With the addition of the box, the temperature reached by the thermocouples increased by about $6.5^{o}\ C$ as compared to the setup with no insulation which a significant improvement. The linear profile is maintained after the initial increment period.

Test 2

In this experiment, the tests were performed using the same power of 3W but different stages of insulation. The same tests were performed at the same stages of insulation as the

previous tests. As expected, the similar improvements were noted as can be seen from the following graphs.

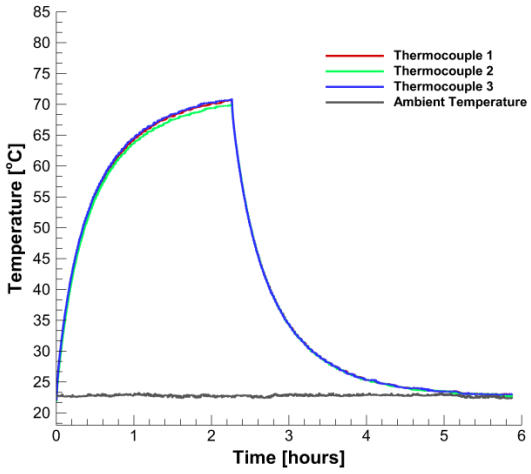

Figure 32: Setup with no insulation

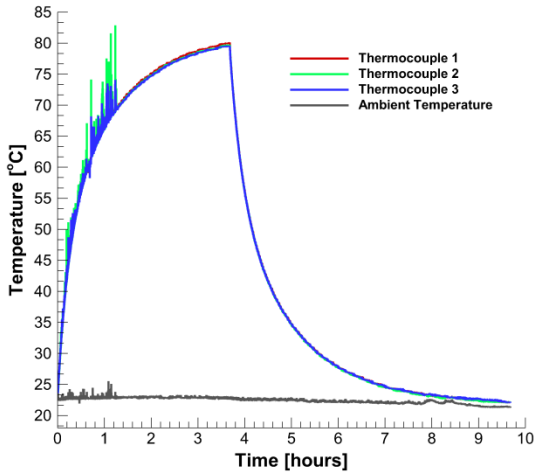

Figure 33: Insulated setup

The graph with the insulation with bubble wrap and box showed significant improvement in the temperature reached by the thermocouples. The increment of the temperature was about $7^o\ C$ which is again a tremendous improvement. But as seen from the graph, the deviations in the thermocouple readings was enormous and unwanted. On inspection, it was seen, that the insulating material was interfering partly with the thermocouple wires and thus we see the significant rise and fall of temperature at the same time from all three thermocouples. The necessary changes were made and the test was run again. The graph clearly shows that the deviations in the thermocouple readings has become negligible

while retaining the insulating effects of the setup. The temperature reached was about $80^{o}\ C$ which is again an improvement of about $8^{0}\ C$ and is a significant.

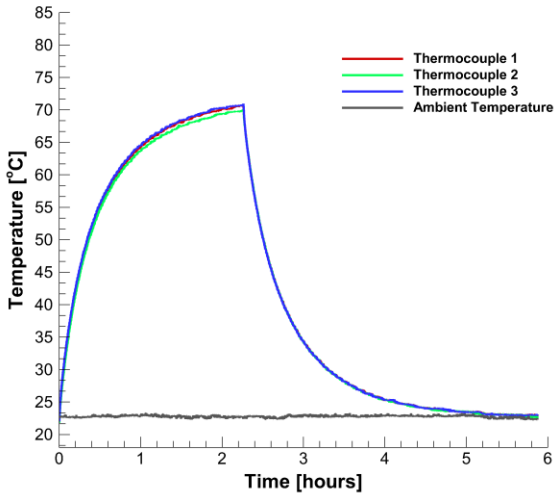

Figure 34: Unchanged setup

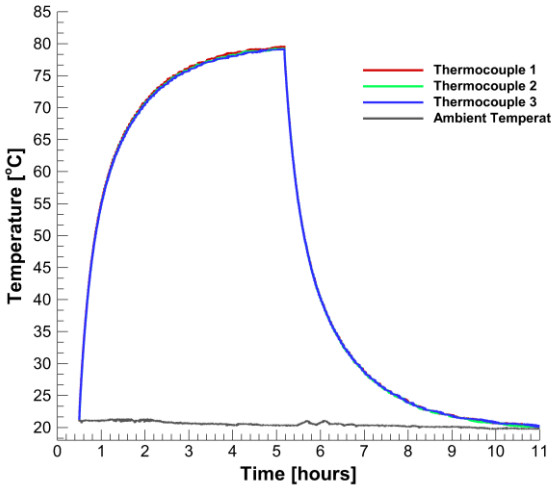

Figure 35: Result after adding insulation

CHAPTER IV

FINAL MODEL

This chapter firstly involves a recap of the problems faced during the tests performed using the wooden setup. It then introduces the new prototype and its various components. Next, the theoretical model on which this technique rests on is discussed in depth. Finally, the results of the all the tests performed using the new setup are discussed in detail, concluding with a few improvements which can be employed in the future to further improve the setup.

The results obtained from the tests performed on the setup clearly were not satisfactory and not up to the mark. The overall goal of the research was to achieve the thermos-physical properties of any test using an economical, robust and accurate measuring technique. The previously described setup was unable to achieve these goals competently and thus, something new needed to be thought of quickly in order to not only get away with all the problems of the previous setup, but also to further improve the accuracy of the results obtained. A few problems pertaining to the previous setup have been discussed in the last section and even after employing techniques to reduce the errors involved, the results were not sufficient. The major problems which could not be solved are as follows:

The first and the most concerning issue was that of the insulation of the setup. The level of insulation required in order to get accurate final results could not be met by the experimental model. Two different layers of insulation of bubble wrap and a cardboard

box were used on the wooden setup and a layer of molten wax was also used to fill up any kind vacant space in order to achieve better layers of insulation. These changes did show some significant improvements as seen in the last section but the scope of improvement was still huge. Moreover, as soon as the power to the heating coil was switched off, the temperature profile dropped rapidly with time which again indicated tremendous heat loss from the setup and a poorly insulated setup.

The next point which was a major drawback of the previously used model was the time taken to achieve a target temperature. As seen from the Temperature vs Time graphs, the temperature took almost five hours to get an increment of about $40^o\ C$ which was a really long time. This was again an indication of the below average insulation of the setup and again this again defeats one of the main purposes of this research of developing a technique which can deliver results quickly and accurately.

The last point which was again a warning indication was the robustness of the setup. Although, at first the wooden setup seemed robust enough, but in fact it was not. The top part of the assembly and the bottom part of the assembly were held together using nuts and bolts. In order to achieve the best insulation possible, a perfect fit was required which could be achieved only if the setup was bolted tightly. But when this task was performed, it lead to a great amount of stress on the setup which either lead to the breaking up of the wooden block or the creation of minor gaps which again defeated the goal of achieving perfect insulation.

Experimental setup

The previously mentioned problems including a few more minor glitches clearly indicated that a new experimental setup was a necessity. The most important issue to be resolved by developing something new was to improve the overall insulation of the setup. This meant reducing the heat loss from the setup to a minimum which could then be verified by visually checking the temperature profile once the power to setup was stopped. Another point to focus was the time taken to achieve a target temperature. This had to be within the order of minutes in order to make the technique feasible for use. Again, the new setup had to be sturdy and rigid so as to not only maintain but further improve the robust factor of the entire setup.

Taking into considerations the previously mentioned factors, the next best insulating material, plastic, was selected as the material to make the base of the entire setup, replacing the previously use wood. Acrylonitrile butadiene styrene (ABS), a common thermoplastic polymer having a chemical formula $(C_8H_8)_x \cdot (C_4H_6)_y \cdot (C_3H_3N)_z$. was the plastic used to develop the model. Again we wanted a material with very low thermal conductivity in order to make sure that the setup was adiabatic in nature. ABS met this necessary condition perfectly as it has a very low thermal conductivity of $0.1\ W/mK$. This ensured that heat loss from the setup was negligible even when the power to heating coil has been cut off. Another important factor in selecting ABS was its excellent toughness, outstanding impact resistance and good stiffness which automatically made the entire setup more sturdy and robust. Moreover, ABS is very easy to machine and

common machining techniques such as turning, drilling, milling, sawing, die-cutting and shearing can be used to make any necessary modification. Additionally, standard shop tools can be used to cut ABS and it can also be line bent with standard heat strips. Another great advantage of using ABS over wood is that it is easy to paint and glue and thus, any changes can be made even after the setup is complete, making it easy to use. ABS is a very light material and therefore, the setup made from can be moved easily, therefore showing its great portability. The following images have been created in Solidworks and show the different parts of the setup both the axial and radial directions. The images on the right column are the Solidworks images while the ones on the left column are the real images of the model. The following images show the axial (Fig. 35, 36, 37, 38) and the radial (Fig. 39, 40, 41, 42) experimental models used.

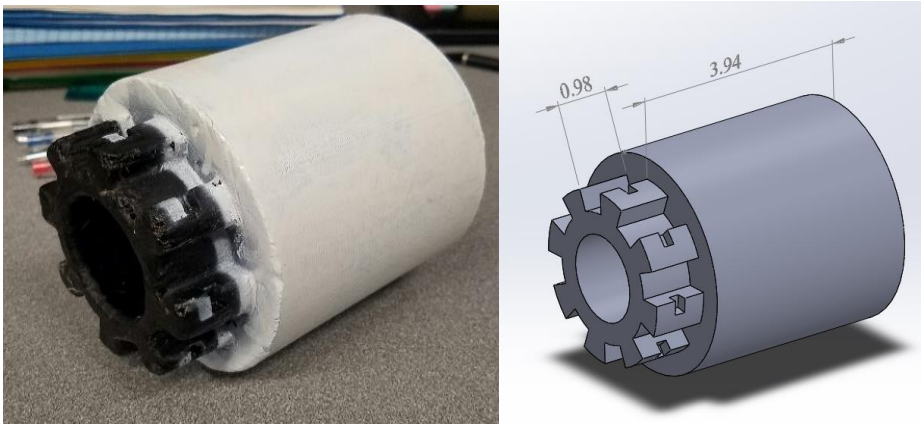

Figure 36: Bottom part of axial assembly

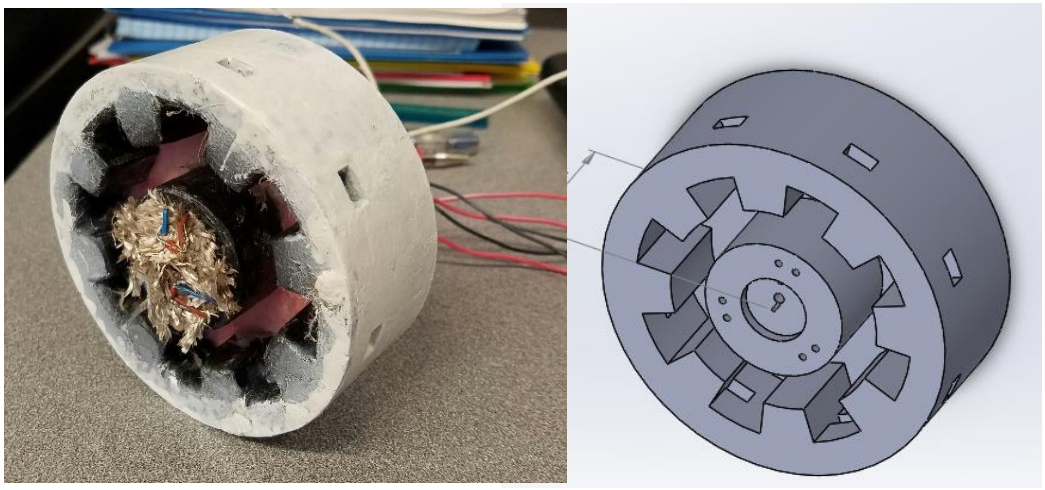

Figure 37: Top part of assembly for axial setup

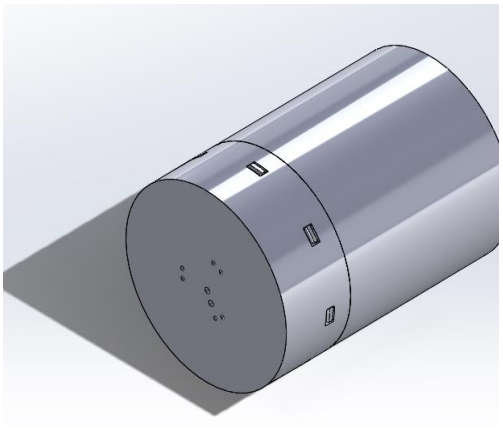

Figure 38: Complete assembly for axial setup

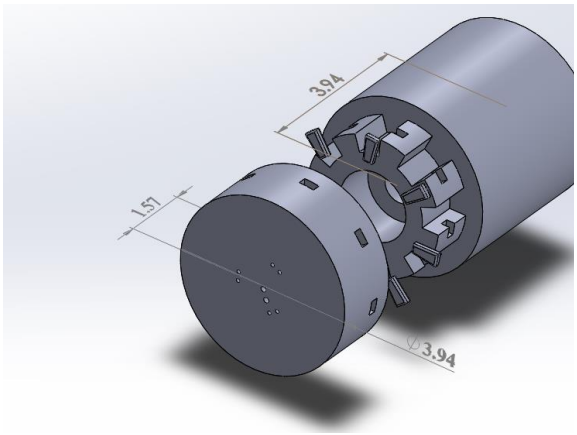

Figure 39: Exploded view of complete axial assembly

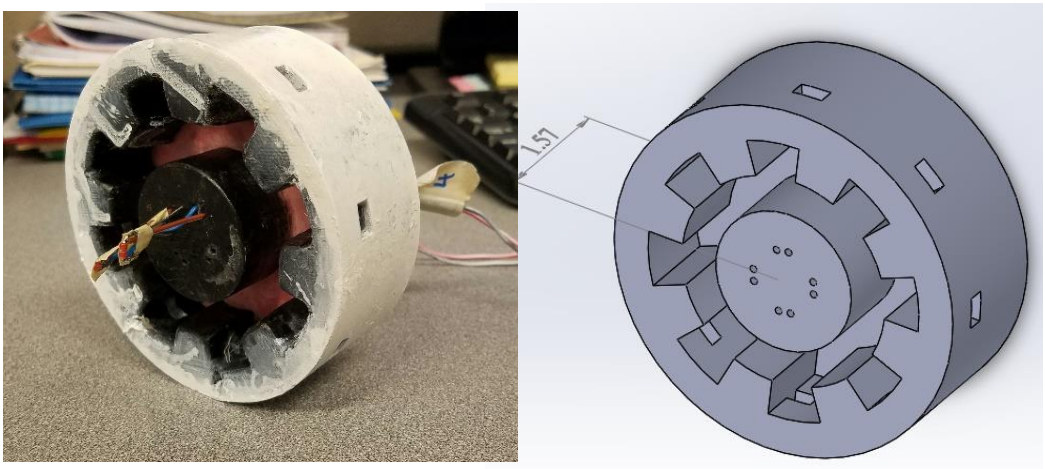

Figure 40: Top part of assembly for radial setup

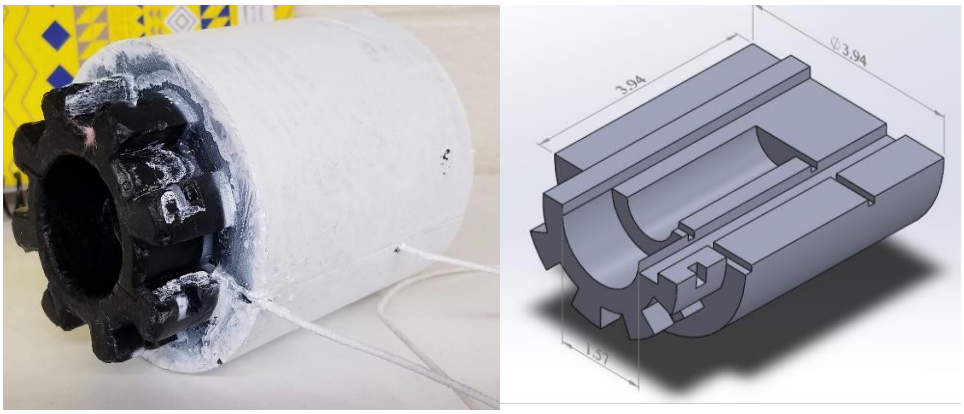

Figure 41: Side view of radial assembly

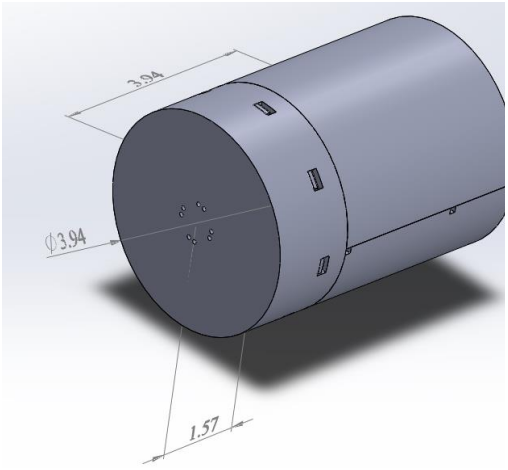

Figure 42: Complete assembly for radial setup

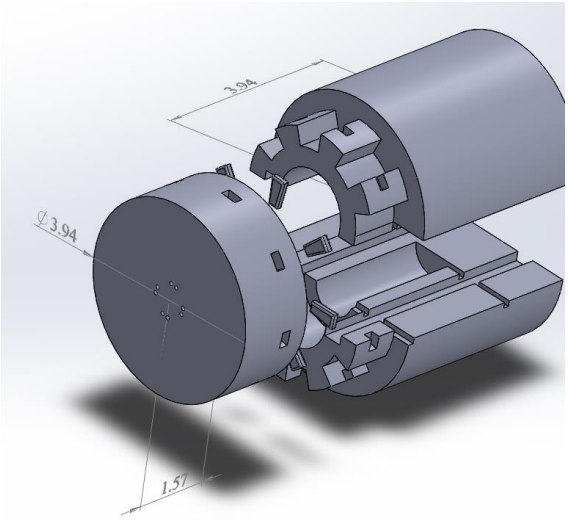

Figure 43: Exploded view of complete radial assembly

The next change which was introduced in the new setup was that of employing of a Thermistor instead of a thermocouple to measure the temperature variations in the cell. The thermistor is a temperature measuring equipment just like the thermocouple and the RTD. Thermistors work on the principle that the electrical resistance of a material changes with temperature which is similar to the principle on which an RTD works. RTDs are made up materials whose resistance increases with increase in temperature. On the contrary, Thermistors are made from certain metal oxides whose resistance decreases with increasing temperature. Thermistors are also called negative temperature coefficient (NTC) devices since their resistance characteristics fall with increasing temperature. The working of a thermistor requires the usage of an instrument across it that measures its

electrical resistance. The resistance then changes with the changing temperature of the thermistor. Subsequently, a table listing the resistance change with temperature can be referred to and the exact value of temperature can be obtained.

Figure 44: Thermistor

A few reasons for using thermistors instead of thermocouples or RTDs have been discussed next. The thermocouples and the RTDs are really expensive equipment whereas the thermistor is really economical and hence was the preferred choice in this research. Moreover, the thermistors react quicker than thermocouples to a change in temperature which again increases the speed at which the temperature is measured and thus improves

the overall efficiency of the setup. Also, the electronic circuitry required for a thermistor is relatively simpler as compared to that of the RTD. Another advantage of thermistors is that they can be produced in very small designs with a fast response and low thermal mass. The last advantage of thermistors over thermocouples is that thermistors don't require any calibration whereas in 90% of cases involving a thermocouple, calibration is a must.

The heating coil was not changed from the previous setup and the same Omegalux rope heater was employed for all the tests performed for the new setup as well. A few changes were made to the heating coil so as to employ the entire length (100% length) of the heating coil so that the amount of heat which goes waste is minimized. This would give better results with less unknown parameters.

The process of measuring an electrical or physical phenomenon such as voltage, current, temperature, pressure, or sound with a computer is called Data acquisition (DAQ). A DAQ system consists of sensors, DAQ measurement hardware, and a computer with programmable software. In our setup, an external 1 $K\Omega$ resistance is applied on the breadboard.

The DAQ board measure the voltage drop across the thermistor used in the setup. It then conditions this data and sends it to the software in the PC attached to the entire setup. The software used in our case to process the data further is the LabVIEW software. Once the data is received by LabVIEW, it converts the voltage into resistance. The relation between

resistance and temperature is then established by calibrating the thermistors. The final relation obtained is as follows:

$$\frac{1}{T} = a + b * log(R_{th})$$

Here, a and b are constants which are obtained through calibration. Once, the values of the constants are found, the resistance data is changed into the temperature data. This gives us the final temperature response as a function of time. The following figure shows the DAQ board used for our experiments.

Figure 45: NI DAQ board

Theoretical model

Imagine a finite sized body completely in equilibrium with the surroundings (i.e., $T\left(\vec{x}, t=0\right) = T_{amb}$) and on the surface of which a heating coil is wrapped around. Assume that at time $t = 0$, the heating coil is turned on. Intuition says that the surface temperature

would increase in time. The increase in surface temperature is both a function of geometric dimensions of the body as well as thermos-physical properties, namely thermal conductivity and heat capacity. Mathematically, the transient heat conduction equation can be solved in the body subject to prescribed heat flux condition to obtain temporal variation of surface temperature[49]. This approach is more commonly referred to as the Forward problem (the problem is to figure out temperature distribution given the material properties and geometric dimensions). The problem can also be contemplated in a reverse manner saying that given the information about surface temperature, thermos-physical properties of the material can be computed. This description is referred to Inverse problem. The mathematics that shoulders the measurement technique presented in this work relies on Inverse problem definition.

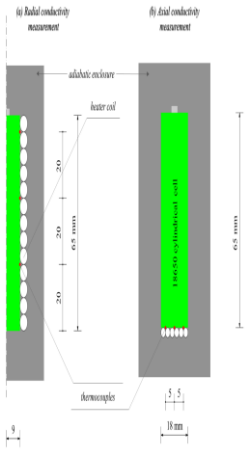

Figure 46: Experimental setup for the radial and axial direction

Radial conduction in 18650 cells

Imagine that a constant heat flux is applied in the radial direction such that there is no variation along the axial (i.e., height) direction. Transient conduction problem for such a configuration assumes the following form:

Governing equation

$$\rho C \frac{\partial T}{\partial t} = \frac{k_r}{r} \frac{\partial}{\partial r}\left(r \frac{\partial T}{\partial r} \right) \tag{1}$$

Boundary conditions

At $r = 0$: $$\frac{\partial T}{\partial r} = 0 \tag{2}$$

At $r = R$: $$k_r \frac{\partial T}{\partial r} = q \tag{3}$$

Initial condition

$$T\left(r, t = 0\right) = 0 \tag{4}$$

Note that the heat flux is assumed to be acting inward. If the cell is initially at a uniform temperature, linearity of the heat conduction equation allows one to redefine temperature as difference between actual and initially uniform value. The derivation outlined hear makes this assumption. This assumption is very easy to realize in practice by suitable choice of cooling period in ambient. Here k_r refers to thermal conductivity in radial direction.

The closed form solution of this problem cannot be obtained using method of separation of variables since it does not have a steady state solution. On the other hand, the method of Laplace transform can be used to convert the parabolic partial differential equation (1) to and ordinary differential equation in s-space[50, 51]. Thus,

$$\mathcal{L}\left\{\frac{\partial T}{\partial t}\right\} = s\mathcal{T}(r) - T(r, t=0) = s\mathcal{T}(r) \tag{5}$$

where $\mathcal{T} = \mathcal{T}(r)$ is the Laplace transform of temperature. Thence, the equivalent problem description in s-space is as follows:

Governing equation

$$s\rho C\mathcal{T} = \frac{k_r}{r}\frac{d}{dr}\left(r\frac{d\mathcal{T}}{dr}\right) \tag{6}$$

Boundary conditions

At $r = 0$: $$\frac{\partial \mathcal{T}}{\partial r} = 0 \tag{7}$$

At $r = R$: $$k_r\frac{\partial \mathcal{T}}{\partial r} = \frac{q}{s} \tag{8}$$

The governing equation in the s-space can be rearranged to give the following form:

$$r^2\frac{d^2\mathcal{T}}{dr^2} + r\frac{d\mathcal{T}}{dr} - \frac{s\rho C r^2}{k_r}\mathcal{T} = 0 \tag{9}$$

Note that equation (9) is similar to the characteristic equation defining modified Bessel functions[52]. Let

$$x^2 = \left(\frac{s\rho C}{k_r} \right) r^2$$

be a new independent variable, then the governing equation along with modified boundary conditions assumes the following form which is identical to the characteristic ordinary differential equation defining the modified Bessel functions $I_0(x)$ and $K_0(x)$.

Governing equation

$$x^2 \frac{d^2\mathcal{T}}{dx^2} + x\frac{d\mathcal{T}}{dx} - x^2\mathcal{T} = 0 \qquad (10)$$

Boundary conditions

At $x = 0$:

$$\frac{d\mathcal{T}}{dx} = 0 \qquad (11)$$

At $x = X$:

$$\frac{d\mathcal{T}}{dx} = \frac{q/s}{k_r\sqrt{s/\alpha_r}} \qquad (12)$$

From the solution of the ordinary differential equation

$$\mathcal{T}(x) = a_1 I_0(x) + a_2 K_0(x) \qquad (13)$$

Since temperature remains bounded and the modified Bessel function of the second kind has a singularity at $x = 0$,

$$a_2 = 0 \tag{14}$$

From identity for modified Bessel function of the first kind, $dI_0(x)/dx = I_1(x)$.

Thence,

$$\frac{d\mathcal{T}}{dx} = a_1 I_1(x) \tag{15}$$

Since, $I_1(x=0) = 0$, the first boundary conditions (Equation (11)) cannot be employed to define the value of a_1. In fact, this boundary condition specifies that the temperature field adopts a finite value at $x = 0$ and in turn justifies for $a_2 = 0$.

From second boundary conditions (Equation (12)):

$$\frac{d\mathcal{T}}{dx} = a_1 I_1(X) = \frac{q/s}{k_r\sqrt{s/\alpha_r}}$$

$$\therefore a_1 = \frac{q/s}{k_r\sqrt{s/\alpha_r}\, I_1(X)} \tag{16}$$

Substituting the value of integration constants a_1 and a_2 in temperature field solution in s-space (Equation (13)):

$$\mathcal{T}(x) = \frac{q/s}{k_r\sqrt{s/\alpha_r}} \cdot \frac{I_0(x)}{I_1(X)} \tag{17}$$

Now one can identify the temperature at the heating coil – cell interface, i.e., $x = X$ (remember that this corresponds to $r = R$).

$$\mathcal{T}(X) = \frac{q/s}{k_r\sqrt{s/\alpha_r}} \cdot \frac{I_0(X)}{I_1(X)} \tag{18}$$

Let us interpret the same problem in state space[53] as if one were to analyze a control system. The boundary heat flux can be conceived as an input signal and the temperature at the boundary as system response (or output) which is characterized by system properties. The output – to – input ratio leads to system impedance specific to the input signal type. The system impedance is a property of the physical dimensions, material properties as well as excitation signal (i.e., input).

Input signal

At $r = R$

$$\mathcal{Q} = \mathcal{L}\{q\} = \frac{q}{s} \tag{19}$$

Output signal

At $r = R$

$$\mathcal{T}(X) = \frac{\mathcal{Q}}{k_r\sqrt{s/\alpha_r}} \cdot \frac{I_0(X)}{I_1(X)} \tag{20}$$

Impedance (output – to – input ratio)

$$\mathcal{Z}(s) = \frac{\mathcal{T}}{\mathcal{Q}} = \frac{1}{k_r\sqrt{s/\alpha_r}} \cdot \frac{I_0\left(R\sqrt{s/\alpha_r}\right)}{I_1\left(R\sqrt{s/\alpha_r}\right)} \tag{21}$$

Note that the impedance response involves material properties k_r, ρ and C, radial dimension R and $s = i\omega$. Thus,

$$\mathcal{Z}(\omega) = \frac{\mathcal{T}}{\mathcal{Q}} = \frac{1}{k_r\sqrt{i\omega/\alpha_r}} \cdot \frac{I_0\left(R\sqrt{i\omega/\alpha_r}\right)}{I_1\left(R\sqrt{i\omega/\alpha_r}\right)} \tag{22}$$

Axial conduction in 18650 cells

The previous discussion outlines the thermal impedance response of 18650 cells for heat flux being applied in radial direction (with uniformity in axial direction). Similarly, the thermal response to heat flux in axial direction would help deconvolve axial thermal conductivity. The problem description with governing equation and corresponding boundary and initial conditions is expressed in equations (23) to (26):

Governing equation

$$\rho C \frac{\partial T}{\partial t} = k_z \frac{\partial^2 T}{\partial z^2} \tag{23}$$

Boundary conditions

At $z = 0$: $$\frac{\partial T}{\partial z} = 0 \tag{24}$$

At $z = H$: $$k_z \frac{\partial T}{\partial z} = q \tag{25}$$

Initial condition

$$T(z, t = 0) = 0 \tag{26}$$

Note that here the non-homogeneous boundary condition is kept at $z = H$ to preserve similarity with radial solution. Depending on the placement of cell with respect to the measurement setup, $z = H$ can coincide either with the cap or the other end.

Following the same procedure as before, equivalent system description in the Laplace domain is as follows:

Governing equation

$$s\rho C\mathfrak{T} = k_z \frac{d^2\mathfrak{T}}{dz^2} \tag{27}$$

Boundary conditions

At $z = 0$: $$\frac{d\mathfrak{T}}{dz} = 0 \tag{28}$$

At $z = H$: $$k_z \frac{d\mathfrak{T}}{dz} = \frac{q}{s} \tag{29}$$

The governing equation (27) can be rearranged to give

$$\frac{d^2\mathfrak{T}}{dz^2} - \left(\frac{s\rho C}{k_z}\right)\mathfrak{T} = 0$$

$$\frac{d^2\mathfrak{T}}{dz^2} - \left(s/\alpha_z\right)\mathfrak{T} = 0 \tag{30}$$

which is a Linear second order ordinary differential equation with constant coefficients, the solution of which can be written as:

$$\mathcal{T}(z) = a_3 \sinh\left(z\sqrt{s/\alpha_z}\right) + a_4 \cosh\left(z\sqrt{s/\alpha_z}\right) \tag{31}$$

Here a's are integration constant which have to be found out using the boundary conditions, while $\sinh(\ ), \cosh(\ )$ correspond to hyperbolic sine and cosine functions[50, 51].

$$\frac{d\mathcal{T}}{dz} = \sqrt{s/\alpha_z}\left\{a_3 \cosh\left(z\sqrt{s/\alpha_z}\right) + a_4 \sinh\left(z\sqrt{s/\alpha_z}\right)\right\} \tag{32}$$

Employing boundary condition at $z = 0$:

$$a_3 = 0 \tag{33}$$

Using another constraint:

$$k_z\sqrt{s/\alpha_z} \cdot a_4 \sinh\left(H\sqrt{s/\alpha_z}\right) = \frac{q}{s}$$

$$a_4 = \frac{q/s}{k_z\sqrt{s/\alpha_z}\sinh\left(H\sqrt{s/\alpha_z}\right)} \tag{34}$$

Thus, the solution of equation (30) subject to boundary conditions (28) and (29) is:

$$\mathcal{T}(z) = \frac{q/s}{k_z\sqrt{s/\alpha_z}} \cdot \frac{\cosh\left(z\sqrt{s/\alpha_z}\right)}{\sinh\left(H\sqrt{s/\alpha_z}\right)} \tag{35}$$

Equivalently the state-space interpretation can be mathematically expressed as follows:

Input signal

At $z = H$

$$\mathcal{Q} = \mathcal{L}\{q\} = \frac{q}{s} \tag{36}$$

Output signal

At $z = H$

$$\mathcal{T}(z) = \frac{\mathcal{Q}}{k_z\sqrt{s/\alpha_z}} \cdot \frac{\cosh\left(H\sqrt{s/\alpha_z}\right)}{\sinh\left(H\sqrt{s/\alpha_z}\right)} \tag{37}$$

Impedance (output – to – input ratio)

$$\mathcal{Z}(s) = \frac{\mathcal{T}}{\mathcal{Q}} = \frac{1}{k_z\sqrt{s/\alpha_z}} \cdot \frac{\cosh\left(H\sqrt{s/\alpha_z}\right)}{\sinh\left(H\sqrt{s/\alpha_z}\right)} \tag{38}$$

In terms of signal frequency, the impedance response assumes the following form:

$$\mathcal{Z}(\omega) = \frac{\mathcal{T}}{\mathcal{Q}} = \frac{1}{k_z\sqrt{i\omega/\alpha_z}} \cdot \frac{\cosh\left(H\sqrt{i\omega/\alpha_z}\right)}{\sinh\left(H\sqrt{i\omega/\alpha_z}\right)} \tag{39}$$

Additional Contributors to Impedance:

1. Heater – thermistor – cell interfacial resistance:

$$Z_i = R_i = \frac{T_{measured} - T_{cell\ surface}}{\ddot{Q}_{cell}}$$

2. Energy Stored in the heating coil

$$C_h \frac{dT_{measured}}{dt} = \ddot{q}_{coil}$$

Taking the Laplace transform:

$$sC_h \mathcal{T}_{measured} = \ddot{Q}$$

Heat flux input to heater: $\ddot{Q} = \ddot{Q}_{\boldsymbol{cell}} + \ddot{Q}_{\boldsymbol{coil}}$

Total Thermal Impedance: $\mathcal{T} = \frac{\mathcal{T}_{measured}}{\ddot{Q}} = \left\{ sC_h + \frac{1}{Z_i + Z_{cell}} \right\}^{-1}$

$$Z = \frac{\mathcal{T}_{measured}}{\ddot{Q}} = \left\{ sC_h + \frac{1}{R_i + 1 \Big/ \left(\pi R^2 k_z \sqrt{\frac{j\omega}{\alpha_z}} tanh\left(H \sqrt{\frac{j\omega}{\alpha_z}} \right) \right)} \right\}^{-1}$$

Tests and results

The tests were performed using a fixed procedure. The following test blocks were used for both the axial and the radial setup:

- Aluminum Block
- 18650 Lithium-ion cell

The following steps were followed while performed the tests:

- A new cell (no capacity fade) with 100 % state of charge was taken. The experiments were performed on the cell in both the radial and axial directions and the resulting temperature vs time data was collected. The following table shows

the details of the current, power and the duration for each experiment performed in both the directions.

Table 4. Conditions used for tests

Direction	**I(mA)**	**Power(W)**	**Time**
Axial	500	2.35	10 min
Radial	250	2.8125	5 min

- Once these tests were over, the cell was discharged at a C/2 rate for about thirty minutes. The state of charge was varied from 100% to 0% at the same C rate for all the tests that were performed.
- Once the cell was discharged, the same thermal impedance tests were repeated in both the radial and the axial directions. This procedure was repeated till the cell was completed discharged.

Table 5. Voltage and SOC

Voltage	SOC
4.13	100%
3.84	75%
3.64	50%
3.56	25%
3.13	0%

- Each test conducted gave us the temperature response with respect to time which was then post processed to give the final results.

Results

The results were obtained by performing the inverse heat transfer technique as mentioned in the previous section. The following steps were followed to reach the final result:

1. The temperature vs time data is used to find the experimental impedance by using a fitting equation. The real part of the impedance and the negative of the imaginary part of the impedance are simultaneously plotted.

2. The theoretical impedance in terms of the thermal diffusivity (α) and the thermal conductivity (k) is calculated using the results generated by utilizing the available governing equations and boundary condition as mentioned in the last section.
3. Curve fitting is performed to obtain the using a fitting function on the theoretical impedance so that it matches with the value of the experimental impedance.
4. The thermal conductivity is found directly from the curve fitting while the heat capacity is calculated using its relation with the thermal diffusivity.

The following graphs were generated for all the tests performed for both the axial and the radial direction. The first graph was generated for the radial direction and it was compared with the temperature time graph previously generated for the Version 1.0. The temperature increment in both the cases is $15^o\ C$. The graphs show a significant difference in the time taken to reach a particular target temperature and also there is a drastic difference in the shape of the plot once the current is stopped. The version 1.0 takes about 50 minutes to reach a temperature increment of $15^o\ C$ whereas it took only about 5 minutes to reach the same temperature increment in the final model. This clearly indicates the superior insulation of the final setup as compared to the previous one. The second thing to note is that once the power is stopped, the temperature drop is drastic in the previous version 1.0 whereas in the final setup, there is a small temperature drop which is attributed to the fact that temperature distribution occurs inside the cell. There is no heat loss to the surroundings in the final setup which shows that the new setup is almost adiabatic in nature.

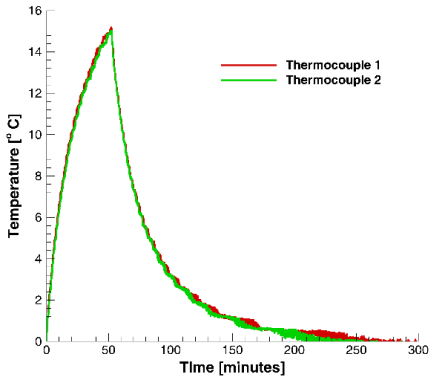

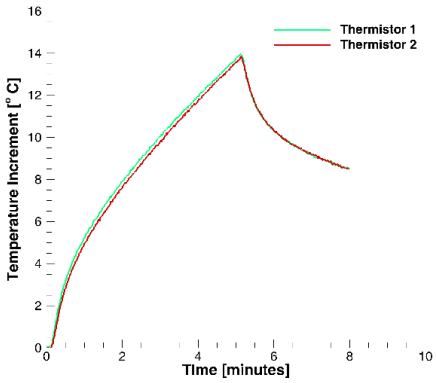

Version 1.0 Final Model

Figure 47 : Radial direction: Target temperature increment =15℃

The next set of graphs were plotted for both the axial and the radial direction with varying state of charge.

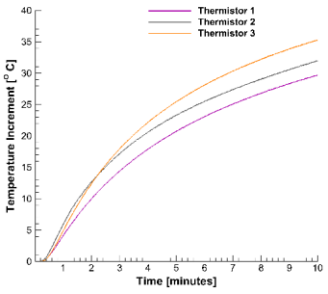

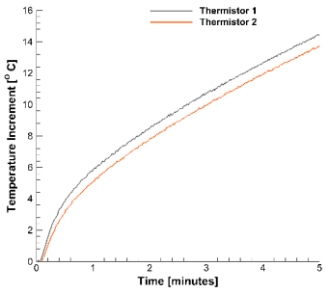

Axial Direction Radial Direction

Figure 48 : State of charge = 100%

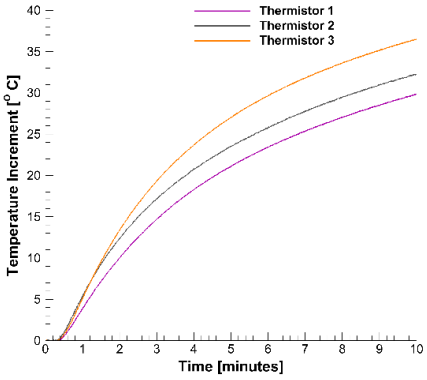

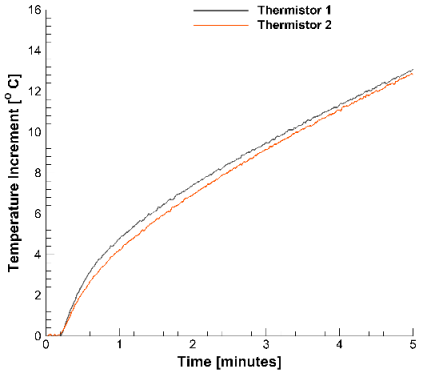

Axial Direction Radial Direction

Figure 49 : State of charge = 75%

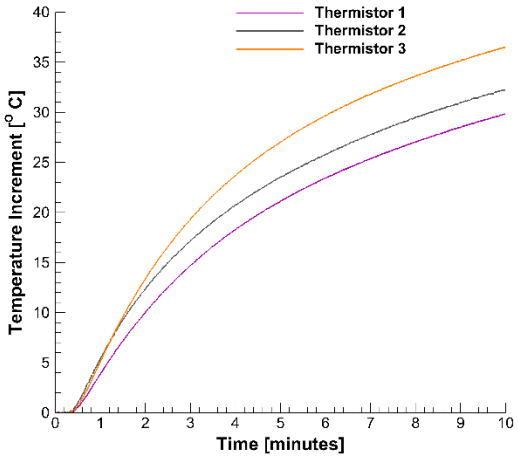

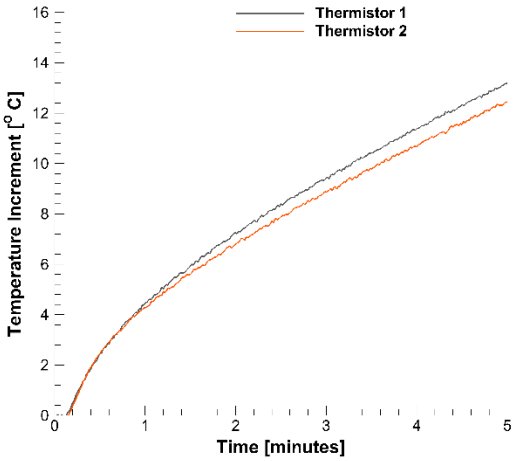

Axial Direction Radial Direction

Figure 50 : State of charge = 50%

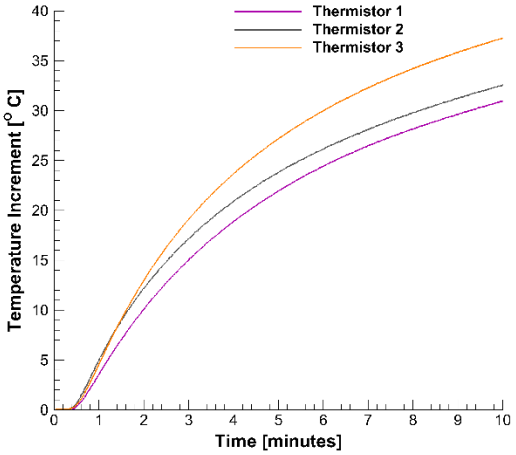

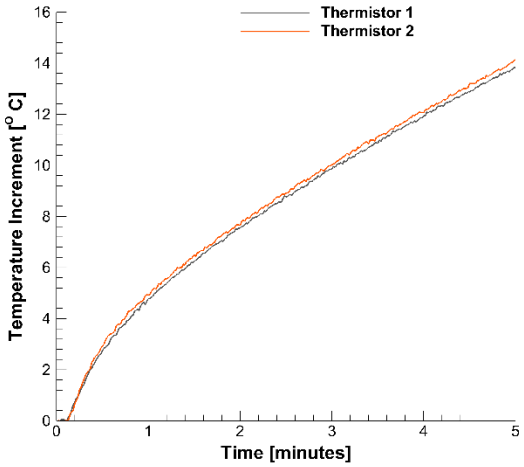

Axial Direction Radial Direction

Figure 51 : State of charge = 25%

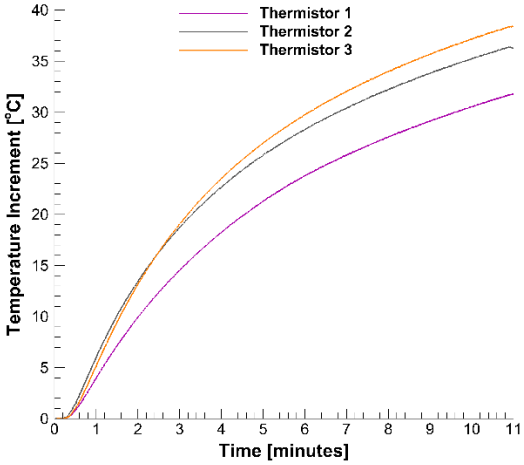

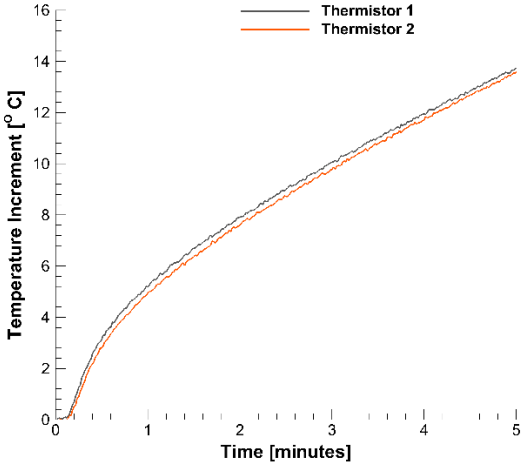

Axial Direction Radial Direction

Figure 52 : State of charge = 0%

Finally, the temperature response for different state of charge of the cell for both the radial direction and the axial direction are plotted in the same plot. The important thing to note is that with changing state of charge of the cell, the temperature response as a function of time does not vary much for both the radial and the axial case.

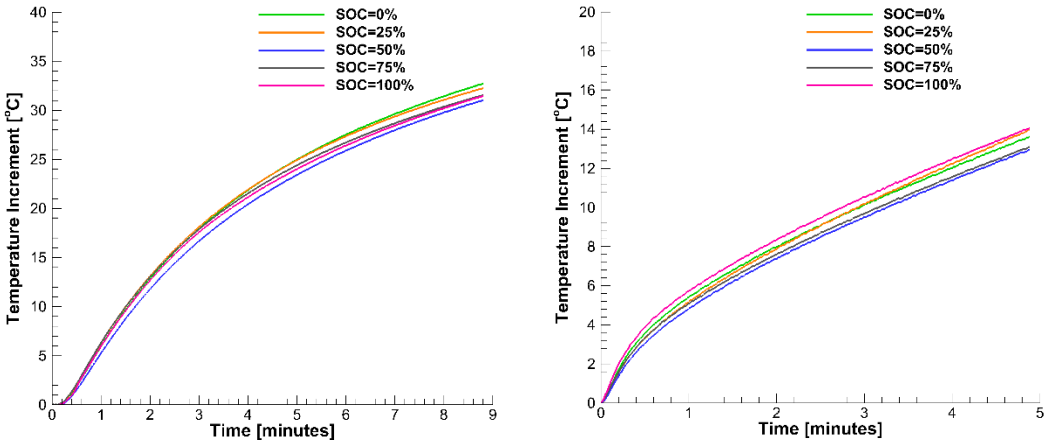

Axial Direction Radial Direction

Figure 53 : Temperature vs time for varying S.O.C

This might lead us to the conclusion that the thermo-physical properties do not vary with state of charge which would be incorrect. Thus, in order to get a better understanding of the dependence of the thermal conductivity and heat capacity of the cell with varying state of charge, the nyquist plots are used. Firstly, the nyquist plots are plotted using the analytical solution derived in the previous section for both the radial and axial direction. The following factors are varied while plotting the graphs:

1. Thermal Conductivity

2. Heat Capacity of the heating coil
3. Volumetric heat capacity of the cell

This was done to study the effect of varying each parameter on the impedance of the cell as seen on the nyquist plot.

The first set of graphs show the effect of changing the thermal conductivity in a particular direction on the total impedance in that direction. All the other parameters such as the heat capacity of the cell, heat capacity of the heating coil etc. are kept constant. The graphs clearly show that with changing the thermal conductivity, the slope of the tail changes drastically. In the axial direction, the values are varied from 0.03 W/Km to 30 W/Km and the corresponding nyquist plots are represented. In the radial direction, the values vary from 0.01 W/Km to 10 W/Km.

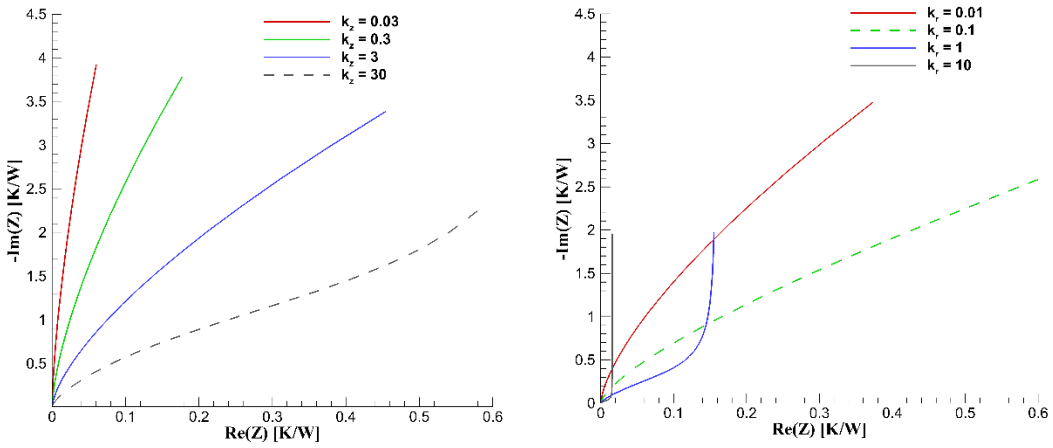

Axial Direction Radial Direction

Figure 54 : Nyquist plot for varying thermal conductivity

The next set of nyquist graphs were plotted with changing heat capacity of the coil. The graphs were plotted with varying the coil heat capacity from 10 J/K to 50 J/K. The graphs clearly show that with changing the value of the heat capacity of the coil, the semicircle of the nyquist plot changes drastically. The point to note is that there is no affect on the tail of the plots with changing the heat capacity of the coil which again corroborates the observation that the tail slope changes only with a change in thermal conductivity.

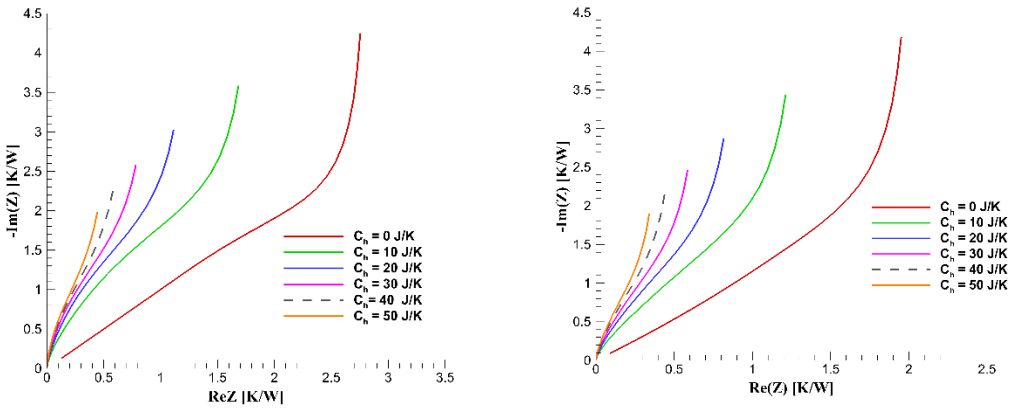

Axial Direction Radial Direction

Figure 55 : Nyquist plot for varying coil heat capacity

The next set of nyquist graphs are plotted with varying the volumetric heat capacity of the cell.

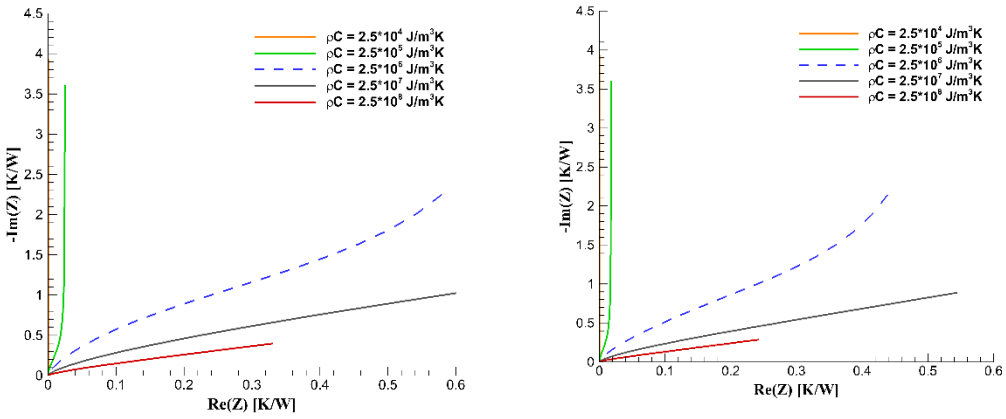

Axial Direction Radial Direction

Figure 56 : Nyquist plot for varying volumetric heat capacity of the cell

Once the trends with varying different parameters are established, the nyquist plots for the experimental thermal impedance are plotted. The following set of nyquist graphs have been plotted with varying state of charge of the cell for both the axial and the radial direction.

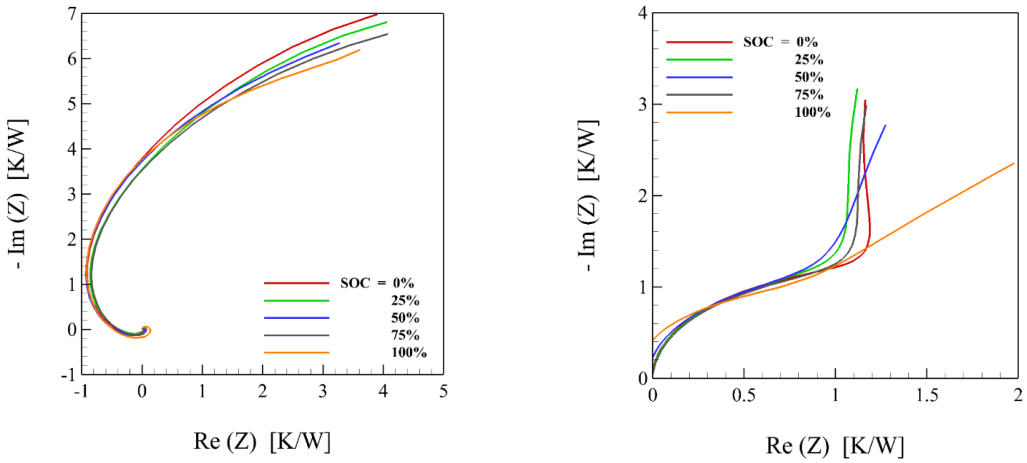

Axial Direction Radial Direction

Figure 57: Nyquist plot for varying state of charge

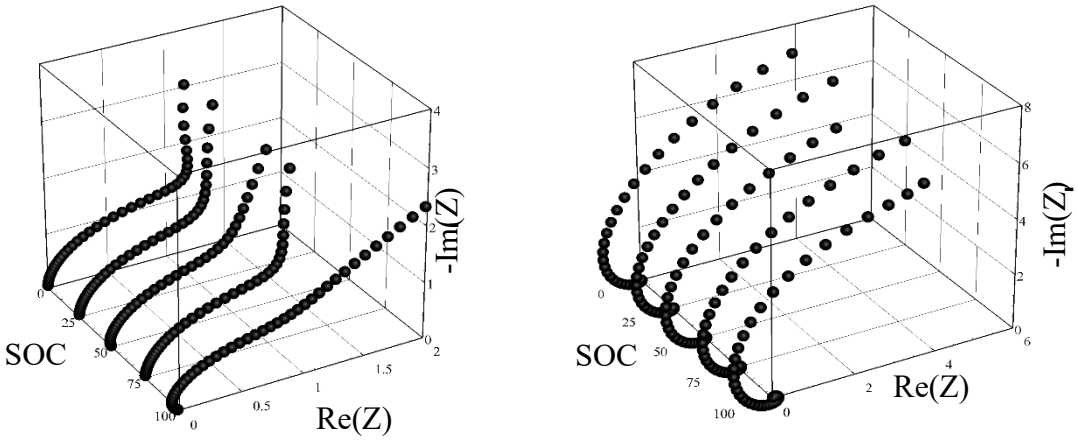

Figure 58: Plot for varying state of charge with varying impedance

The above graphs are analyzed with the pre-established trends as obtained in the previous section. The nyquist plot for the axial direction does not show any significant variation with changing the state of charge of the cell indicating that the axial thermal conductivity is relatively independent of the state of charge of the cell. The radial nyquist plot on the other shows a drastic difference. The semicircle region of the nyquist plot remains almost the same for the radial direction as expected since the heating coil remains constant for all the tests. The tail region, however, shows a significant difference with changing SOC of the cell clearly indicating the change in the radial thermal conductivity with discharging of the cell.

CHAPTER V

SUMMARY AND CONCLUSIONS

Summary

The previous works, the proposed models were all precursors to the development of the final technique. The new proposed technique presented in this research is a quick, non-invasive and robust technique to obtain the thermo-physical properties of any material with the dimensions similar to that of an 18650 lithium-ion cell. This final model presented here takes into consideration all the various contributors which might lead to a change in the thermal conductivity and heat capacity of the test block and thus, the results obtained are more accurate than any of the previous techniques mentioned in the literature review. A few highlighting points were also observed as a part of the experiments performed and during the post processing of the experimental data. The first major observation which finally led to the development of the new technique was that the time space is not a suitable domain to perform the experiments and the calculations. Observations and the calculations performed in the time domain do not show any significant results. Thus, the frequency space is a more apt domain to perform all the experiments and the post process analysis. The major advantages observed while working in the frequency domain were that in this domain, the systems are easily employ corrective measurements for noise disturbances generated during the experiments which would not have been possible in the time domain. Another great advantage of the frequency space is that the variation in parameters is more easily determined in this domain as compared to the time domain. Convincing variations are seen in the nyquist plots with varying state of charge of the cell when the calculations

are performed in the frequency domain and thus proving that this is a more suitable and reliable approach. The experimental plots clearly show the difference in the cell impedance in the axial and the radial direction which corroborates the fact that anisotropy exists in the cell. The results clearly indicate that the thermal conductivity in the axial direction is independent of state of charge which in sync with our intuition as the current would take the path of least resistance and thus pass through the current collectors rather than through the electrodes. On the other hand, a significant drop in thermal conductivity is observed in the radial direction with discharge of the cell which again is a logical conclusion since the lithiation and delithiation process leads to an increase in impedance in the radial direction which leads to the observed drop in conductivity. Thus, this technique is a quick, reliable, robust, non-invasive and economical method of obtaining the thermo-physical properties of an 18650 lithium-ion cell.

Future scope

The experiments performed in this technique have been on a fresh 18650 lithium-ion cell. The next step would be to use a degraded cell with capacity fading and run the same tests in order to find the trend of the thermo-physical properties with capacity fading. Moreover, the effects of varying the cell chemistry on the thermal conductivity and heat capacity can also be studied in the future. Additionally, cells of different manufacturers can be tested under similar conditions to find the thermal conductivity and heat capacity of each of them. Finally, the setup presented in this technique is useful for any material with the dimensions of that of an 18650 cell but in the future, this can be extended to accommodate a 26650 cell and also a pouch cell.

REFERENCES

[1] S. B. Company. (1999). *SONY LIP-4WM ('Gumstick' Sony LIP4WM, LIP-4WM)*. Available: http://www.smallbattery.company.org.uk/sbc_lip4wm.htm

[2] Libretexts. (2017). *Electrochemical Energy Storage and Conversion*. Available: https://chem.libretexts.org/Textbook_Maps/General_Chemistry_Textbook_Maps/Map%3A_Chem1_(Lower)/24%3A_Electrochemistry/24.6%3A_Electrochemical_Energy_Storage_and_Conversion

[3] L. Shenzhen Ding Tai Battery Co. (1999). *Prismatic Lithium Iron Phosphate Battery Cell 3.2V 8Ah LiFePO4 Punch Cell*. Available: http://dtbattery.en.alibaba.com/product/60082732935-800427731/prismatic_lithium_iron_phosphate_battery_cell_3_2V_8Ah_LiFePO4_punch_cell.html1999

[4] M. corporation. (1994). *3mm Width Aluminum Tab as Positive Terminal for Pouch Li-ion Cell* Available: http://www.mtixtl.com/3mmAluminumTabasPositiveTerminalforPolymerLi-ionBattery40pcs/Box.aspx

[5] Wikipedia. (2017). *Lithium Ion Battery*. Available: https://en.wikipedia.org/wiki/Lithium-ion_battery

[6] V. P. E. R. V. Group. (2016). *The Lithium-ion Battery*. Available: https://engineering.purdue.edu/ViPER/research.html

[7] A. C. Ltd. (2015). *Lithium Ion Battery Advantages & Disadvantage*. Available: http://www.radio-electronics.com/info/power-management/battery-technology/lithium-ion-battery-advantages-disadvantages.php

[8] R. Show. (2017). *The 2017 Chevrolet Bolt's Electric Powertrain*. Available: https://www.cnet.com/roadshow/news/deep-dive-2017-chevrolet-bolt-electric-powertrain/

[9] C. Doctors. (2016). *Self Discharge of Batteries*. Available: http://corrosion-doctors.org/Batteries/self-compare.htm

[10] E. M. Grant A. Umeda, Monique Richard, Kimber L. Stamm, Fred Wudlc and Bruce Dunn, "Protection of lithium metal surfaces using tetraethoxysilane," *Journal of Materials Chemistry*, 8th October 2010.

[11] COMSOL. (2017). *How to Model Short Circuits in Lithium-Ion Batteries*. Available: https://www.comsol.com/blogs/how-to-model-short-circuits-in-lithium-ion-batteries/

[12] W. C. Ltd. (2005). *Lithium Battery Failures*. Available: http://www.mpoweruk.com/lithium_failures.htm

[13] Wikipedia. (2017). *Thermal Runaway*. Available: https://en.wikipedia.org/wiki/Thermal_runaway

[14] A. T. LLC. (2014). *Prevent Thermal Runaway Propagation*. Available: https://www.allcelltech.com/index.php/technology/pcc-thermal-management/prevents-thermal-runaway

[15] V. Woollaston. (2015). *Watch a Battery EXPLODE and Release Jets of Molten Liquid into the Air: Thermal Images Capture What Happens When a Cell Overheats*. Available: http://www.dailymail.co.uk/sciencetech/article-3059176/Watch-battery-EXPLODE-release-jets-molten-liquid-air-Thermal-images-capture-happens-cell-overheats.html

[16] M.R. Khan, S.J. Andreasen, and S.K. Kaer, "Novel battery thermal management system for greater lifetime ratifying current quality and safety standard." *Battery Connections,* vol. 2014, pp. 6-10, 2014.

[17] S. Drake, D. Wetz, J. Ostanek, S. Miller, J. Heinzel, and A. Jain, "Measurement of anisotropic thermophysical properties of cylindrical Li-ion cells," *Journal of Power Sources*, vol. 252, pp. 298-304, 2014.

[18] X. Zhang, "Thermal analysis of a cylindrical lithium-ion battery," *Electrochimica Acta*, vol. 56, no. 3, pp. 1246-1255, 2011.

[19] Y. Chen and J. W. Evans, "Thermal analysis of Lithium- Ion batteries," *Journal of the Electrochemical Society*, vol. 143, no. 9, pp. 2708-2712, 1996.

[20] T. Hatchard, D. MacNeil, A. Basu, and J. Dahn, "Thermal model of cylindrical and prismatic lithium-ion cells," *Journal of The Electrochemical Society,* vol. 148, no. 7, pp. A755-A761, 2001.

[21] S. A. H. Hossein Maleki, J. Robert Selman, Ralph B. Dinwiddie, H. Wangb, "Thermal Properties of Lithium- Ion Battery and Components," *Journal of The Electrochemical Society,* vol. 146 (3) 947-954, 1999.

[22] N. Sato, "Thermal behavior analysis of lithium-ion batteries for electric and hybrid vehicles," *Journal of Power Sources,* vol. 99, no. 1, pp. 70-77, 2001.

[23] C. R. Pals and J. Newman, "Thermal modeling of the lithium/polymer battery II. Temperature profiles in a cell stack," *Journal of the Electrochemical Society,* vol. 142, no. 10, pp. 3282-3288, 1995.

[24] T. F. F. Marc Doyle, John Newman, "Modeling of Galvanostatic Charge and Discharge of the Lithium/Polymer/Insertion Cell," *J. Electrochem. Soc. ,* vol. 140, no. 6, 1993.

[25] D. Bernardi, E. Pawlikowski, and J. Newman, "A general energy balance for battery systems," *Journal of the Electrochemical Society,* vol. 132, no. 1, pp. 5-12, 1985.

[26] S. Al Hallaj, H. Maleki, J. S. Hong, and J. R. Selman, "Thermal modeling and design considerations of lithium-ion batteries," (in English), *Journal of Power Sources,* vol. 83, no. 1-2, pp. 1-8, Oct 1999.

[27] S. Chacko and Y. M. Chung, "Thermal modelling of Li-ion polymer battery for electric vehicle drive cycles," *Journal of Power Sources,* vol. 213, pp. 296-303, 9/1/ 2012.

[28] L. Saw, Y. Ye, and A. Tay, "Electrochemical–thermal analysis of 18650 lithium iron phosphate cell," *Energy Conversion and Management,* vol. 75, pp. 162-174, 2013.

[29] A. Eddahech, O. Briat, and J.-M. Vinassa, "Thermal characterization of a high-power lithium-ion battery: Potentiometric and calorimetric measurement of entropy changes," *Energy*, vol. 61, pp. 432-439, 2013.

[30] H. Badenhorst and C. Sandrock, "Novel method for thermal conductivity measurement through flux signal deconvolution," *Journal of Energy Storage*, vol. 6, pp. 32-39, 2016.

[31] J. Klett, R. Hardy, E. Romine, C. Walls, and T. Burchell, "High-thermal-conductivity, mesophase-pitch-derived carbon foams: effect of precursor on structure and properties," *Carbon*, vol. 38, no. 7, pp. 953-973, 2000.

[32] A. Franco, "An apparatus for the routine measurement of thermal conductivity of materials for building application based on a transient hot-wire method," *Applied Thermal Engineering*, vol. 27, no. 14, pp. 2495-2504, 2007.

[33] J. Blackwell, "A transient- flow method for determination of thermal constants of insulating materials in bulk part I—Theory," *Journal of Applied Physics*, vol. 25, no. 2, pp. 137-144, 1954.

[34] B. Belkerk, M. Soussou, M. Carette, M. Djouadi, and Y. Scudeller, "Measuring thermal conductivity of thin films and coatings with the ultra-fast transient hot-strip technique," *Journal of Physics D: Applied Physics*, vol. 45, no. 29, p. 295303, 2012.

[35] G. A. Slack and V. G. Tsoukala, "Some properties of semiconducting IrSb3," *Journal of Applied Physics*, vol. 76, no. 3, pp. 1665-1671, 1994.

[36] S.-M. Lee, D. G. Cahill, and R. Venkatasubramanian, "Thermal conductivity of Si–Ge superlattices," *Applied Physics Letters*, vol. 70, no. 22, pp. 2957-2959, 1997.

[37] S. Orain, Y. Scudeller, and T. Brousse, "Structural and microstructural effects on the thermal conductivity of zirconia thin films," *Microscale Thermophysical Engineering*, vol. 5, no. 4, pp. 267-275, 2001.

[38] C. Mikolajczak, M. Kahn, K. White, and R. T. Long, *Lithium-ion batteries hazard and use assessment*. Springer Science & Business Media, 2012.

[39] T. M. Bandhauer, S. Garimella, and T. F. Fuller, "A critical review of thermal issues in lithium-ion batteries," *Journal of the Electrochemical Society,* vol. 158, no. 3, pp. R1-R25, 2011.

[40] A. A. Pesaran, "Battery thermal management in EV and HEVs: issues and solutions," *Battery Man,* vol. 43, no. 5, pp. 34-49, 2001.

[41] A. Y. Cai, Li-ping Chen, Jiang-ping Xi, Tong-geng Xin, Shi-gang Wu, Wei, "Thermal conductivity of anodic alumina film at (220 to 480) K by laser flash technique," *Journal of Chemical & Engineering Data,* vol. 55, no. 11, pp. 4840-4843, 2010.

[42] E. Barsoukov, J. H. Jang, and H. Lee, "Thermal impedance spectroscopy for Li-ion batteries using heat-pulse response analysis," *Journal of Power Sources,* vol. 109, no. 2, pp. 313-320, 2002.

[43] M. Fleckenstein, S. Fischer, O. Bohlen, and B. Bäker, "Thermal Impedance Spectroscopy-A method for the thermal characterization of high power battery cells," *Journal of Power Sources,* vol. 223, pp. 259-267, 2013.

[44] K. Shah, V. Vishwakarma, and A. Jain, "Measurement of Multiscale Thermal Transport Phenomena in Li-Ion Cells: A Review," *Journal of Electrochemical Energy Conversion and Storage,* vol. 13, no. 3, p. 030801, 2016.

[45] OMEGA. (2003). *Thermocouples*. Available: http://www.omega.com/prodinfo/thermocouples.html

[46] Wikipedia. (2017). *Thermocouple*. Available: https://en.wikipedia.org/wiki/Thermocouple

[47] K. E. LTD. (1995). *Flexible Rope Heaters*. Available: http://www.korel.com.tr/products_1a.htm

[48] O. Engineering. (2003). *OMEGALUX® Rope Heaters*. Available: http://www.omega.com/pptst/FGR.html

[49] M. N. Ozisik, *Heat conduction*. John Wiley & Sons, 1993.

[50] M. D. Greenberg, *Advanced engineering mathematics*. Prentice-Hall, 1988.

[51] E. Kreyszig, *Advanced engineering mathematics*. John Wiley & Sons, 2010.

[52] T. L. Bergman, F. P. Incropera, D. P. DeWitt, and A. S. Lavine, *Fundamentals of heat and mass transfer*. John Wiley & Sons, 2011.

[53] J. Durbin and S. J. Koopman, *Time series analysis by state space methods* (no. 38). Oxford University Press, 2012.